Royal Netherlands
Meteorological Institute
Ministry of Infrastructure and the Environment

Evaluation of Meteosat-derived surface solar radiation and its dependence on aerosol properties

Xun Wang

KNMI Internal Report IR-2017-01

Koninklijk Nederlands
Meteorologisch Instituut
Ministerie van Infrastructuur en Milieu

WAGENINGEN
UNIVERSITY & RESEARCH

INTERNSHIP PROJECT REPORT

Evaluation of Meteosat-derived surface solar radiation and its dependence on aerosol properties

Author: **Xun WANG**
Date: **August 9, 2017**

Supervisor(s): **Jan Fokke MEIRINK**
Institute: **Koninklijk Nederlands Meteorologisch Instituut (KNMI)**
Department: **R&D Satellite Observations (RDSW)**
Address: **Utrechtseweg 297**
3731 GA De Bilt
the Netherlands

Abstract

As one of the most mature resources to generate electricity among the renewable power, the demand for solar energy is growing constantly. Accurate solar irradiance data is crucial for successful photovoltaic application. In this context, RDSW is retrieving surface solar irradiance from Meteosat satellite observations using the CPP-SICCS algorithm. Appropriate processing of satellite observations provides accurate spatially continuous solar irradiance over vast territories with high temporal resolution. In this project, investigations on solar irradiance data retrieved by satellite instruments are carried out in three levels. The first is to compare aerosol properties, one of the most important factors in deriving solar radiation for cloud-free conditions, from three different datasets. Aerosol datasets show high consistency and their input in CPP-SICCS algorithm also delivers very similar results. The next is to evaluate an updated version of CPP-SICCS by making comparison with the current operational version. About 20 % difference in cloud phase identification is found between two versions. Changes in surface solar radiation are overall small except for ice clouds. Finally a case study of the IJsselmeer area focusing on both satellite observations and ground-based measurements is performed. The results show that more clouds retrieved over the lake area lead to lower radiation. The CPP-SICCS surface radiation observations are highly consistent with measurements at the KNMI stations around the IJsselmeer lake. In contrast, temporary measurements performed at Houtribdijk (a dike crossing the lake) turn out to be of insufficient quality to identify potential satellite retrieval biases over the lake.

Keywords:
Surface solar irradiance; Aerosol properties; Satellite observation; Meteosat

Contents

1 Introduction **1**
- 1.1 Background . . . 1
- 1.2 Description of datasets and algorithms . . . 1
  - 1.2.1 Aerosol property datasets . . . 1
  - 1.2.2 CPP-SICCS product . . . 2
- 1.3 Knowledge gap . . . 4
- 1.4 Objective and research questions . . . 4
- 1.5 Outline . . . 4

2 Methodology **5**
- 2.1 Inter-comparison of aerosol property datasets . . . 5
  - 2.1.1 Comparison of aerosol property datasets . . . 5
  - 2.1.2 Effect of different aerosol properties inputs on clear sky solar radiation using MSG-CPP algorithm . . . 5
- 2.2 Comparison between new and old version of CPP-SICCS product . . . 6
  - 2.2.1 Data attributes . . . 6
  - 2.2.2 Data analysis . . . 6
- 2.3 Case study: Investigation on a special case of IJsselmeer area . . . 6
  - 2.3.1 Data attributes . . . 6
  - 2.3.2 Data processing & analysis . . . 8

3 Results & discussions on inter-comparison of aerosol datasets **9**
- 3.1 Comparison of aerosol property datasets . . . 9
  - 3.1.1 Global Area . . . 9
  - 3.1.2 European Area . . . 11
- 3.2 Effect of different aerosol properties inputs on clear sky solar irradiance using MSG-CPP algorithm . . . 13
  - 3.2.1 MSG full disk area . . . 13
  - 3.2.2 European Area . . . 14

4 Results & discussions on CPP-SICCS algorithm **16**
- 4.1 MSG full disk area . . . 16
  - 4.1.1 9 scenarios by cloud phase identification . . . 16
  - 4.1.2 Statistical analysis . . . 18
- 4.2 European area . . . 18
  - 4.2.1 9 scenarios by cloud phase identification . . . 18
  - 4.2.2 Statistical analysis . . . 18

5 Results & discussion on case study in IJsselmeer area **21**
- 5.1 CPP-SICCS satellite observations . . . 21
- 5.2 Ground Measurements . . . 21
  - 5.2.1 Elimination of problematic data of Houtribdijk measurements . . . 21
  - 5.2.2 Comparison among ground measurements . . . 23
- 5.3 Aggregated satellite observations . . . 25
- 5.4 Ground measurements versus satellite observations . . . 25

6 General discussion **28**

7 Conclusion **29**

Acknowlegements **30**

Appendix A Supplementary figures **33**

Nomenclature and Abbreviations

AOT_{500}	aerosol optical thickness at wavelength of 500 nm
SDS	surface downwelling solar radiation [W/m^2]
SDS_{cs}	clear-sky surface downwelling solar radiation [W/m^2]
A_{exp}	Ångström exponent
CAMS	Copernicus Atmosphere Monitoring Service
CPP	Cloud Physical Properties algorithm
ECMWF	European Centre for Medium-Range Weather Forecasts
MACC	Monitoring Atmospheric Composition and Climate project
MSG	Meteosat Second Generation satellite
SEVIRI	Spinning Enhanced Visible and InfraRed Imager
SICCS	Surface Insolation under Clear and Cloudy skies derived from SEVIRI imagery algorithm

Chapter 1 Introduction

1.1 Background

The constantly growing energy consumption has already raised concerns on insufficient energy supply, exhaustion of natural resources and severe environmental impacts. The International Energy Agency (IEA) published a set of statistical data showing that there was a 102% growth of total consumption of fuel during the last 40 years (1973 - 2014) corresponding to an average annual increase of 1.8 % [1]. Solar power has been used as an alternative to fossil fuel since the oil crisis of the early 1970s owing to its sustainable, non-polluting characteristics. Compared to a diesel engine generator of comparable capacity, although a photovoltaic (PV) system usually has higher capital investments, the operating and maintenance costs are always lower [2]. However, the strong dependence on meteorological conditions increases the difficulty for PV energy supply and storage[3]. Accurate and spatially distributed data on surface downwelling solar radiation (SDS) are crucial for photovoltaic application [4]. Besides ground meteorological stations, spatially continuous irradiance can also be derived directly from meteorological geostationary satellites (e.g. Meteosat) [5, 6, 7]. Processing of satellite observations provides solar radiation data over vast territories with high temporal resolution [8].

Koninklijk Nederlands Meteorologisch Instituut (KNMI, Dutch for: Royal Netherlands Meteorological Institute) is the national research and information centre for meteorology, climate, air quality and seismology [9]. The Research & Development Satellite observation department (RDSW) at KNMI studies the composition and dynamics of the global atmosphere using satellite observations. One of the themes of RDSW is to study about clouds, aerosols and radiation. Every 15 minutes satellite instruments take detailed pictures of the earth, both from visible and infrared light. In the RDSW department these images are used to derive information about cloudiness, precipitation, and solar radiation. These data are important for investigating variations and trends in cloudiness and moreover, the data are used for various practical applications, such as monitoring the efficiency of solar panels.

Clouds are strong regulators of the Earth's radiative balance, and play a key role in the hydrological cycle by determining precipitation and evaporation [10]. Cloud physical properties are the factor that dominates the calculation of atmospheric transmission of solar radiation [6]. Aerosols are an important component of air pollution and affect the radiative balance of the Earth. According to [11], changes in solar radiation are attributed to not only clouds, but also aerosols. For instance, observations from the Indian Ocean Experiment show that absorbing aerosols from human activities can spread over large areas of the Indian Ocean and reduce SDS by about 7 % over the entire northern Indian Ocean [12]. Furthermore, aerosol-cloud interactions also contribute to additional large-scale changes in the surface solar radiation[13].

These two most influential factors determine the accuracy of satellite observation products. Errors in the temporal or spatial distribution of clouds or aerosols can cause large errors in SDS calculations [6]. Thus relevant parameters of clouds and aerosols play a crucial roles in this study.

1.2 Description of datasets and algorithms

The background and introduction of relevant aerosol datasets and algorithms is given in this section.

1.2.1 Aerosol property datasets

Monitoring Atmospheric Composition and Climate (MACC) reanalysis

Monitoring Atmospheric Composition and Climate (MACC) is a research project aimed at establishing the core global and regional atmospheric environmental services for the European Global Monitoring

for Environment and Security (GMES) initiative. A reanalysis of atmospheric composition data covering the period 2003-2010 was constructed as part of the MACC project by assimilating satellite data into a global model and data assimilation system. The global model and data assimilation system was based on the Intergrated Forecast System (IFS) of the European Centre for Medium-Range Weather Forecasts (ECMWF). The reanalysis provides fields of chemically reactive gases including carbon monoxide, ozone, nitrogen oxides, and formaldehyde, as well as aerosols and greenhouse gases globally in a spatial resolution of about 80 km [14].

Copernicus Atmosphere Monitoring Service (CAMS) interim reanalysis

CAMS interim reanalysis is a new reanalysis dataset of atmospheric composition for the period 2003-2015 produced by Copernicus Atmosphere Monitoring Service (CAMS). Satellite observations of reactive gases, ozone and aerosols properties have been assimilated with the IFS of ECMWF as well. It provides products with resolution of about 110 km [15].

CAMS operational run

This is the operational atmospheric composition forecasting product developed by CAMS. Unlike MACC and CAMS interim reanalysis as fixed models, upgrades have been made to the operational run over time, which is available in near-real time. Currently, the resolution is 40 km [16].

In this report, MACC reanalysis, CAMS interim reanalysis and CAMS operational run datasets are referred as 'MACC', 'eac3' and '0001' respectively, following the terminology from the ECMWF archiving centre.

1.2.2 CPP-SICCS product

The main product used for data retrieval and SDS calculation in this study is CPP-SICCS. The principle diagram is shown in Figure 1.1.

Meteosat Second Generation (MSG) is a series of geostationary satellites positioned near 0 degree longitude. It carries an instrument, the Spinning Enhanced Visible and InfraRed Imager (SEVIRI), which observes the Earth in 12 spectral channels and provides full disc imagery every 15 minutes [17]. The images retrieved from SEVIRI are classified into clear or cloudy pixels by a cloud mask procedure [18].

For cloudy pixels, the Cloud Physical Properties (CPP) algorithm [19] uses SEVIRI's VIS and near-infrared (NIR) measurements to retrieve cloud optical thickness (τ) and cloud particle effective radius (r_e). CPP is based on lookup tables (LUTs) of top-of-atmosphere reflectances for single-layer, plane-parallel water and ice clouds, simulated by the Doubling Adding KNMI (DAK) radiative transfer model [20, 21]. For cloudy pixels τ and r_e are retrieved by matching the observed reflectance to the LUTs. First the ice cloud LUT is tried. If this leads to a match and if the cloud top temperature - retrieved from the 10.8 μm channel - is below 265 K, the thermodynamic phase is set to ice. Otherwise, the water cloud LUT is used, and the phase is set to liquid.

For clear pixels aerosol properties from ECMWF are taken. The parameters from both clear and cloudy pixels enter the Surface Insolation under Clear and Cloudy skies derived from SEVIRI imagery (SICCS) algorithm to produce surface solar radiation [6].

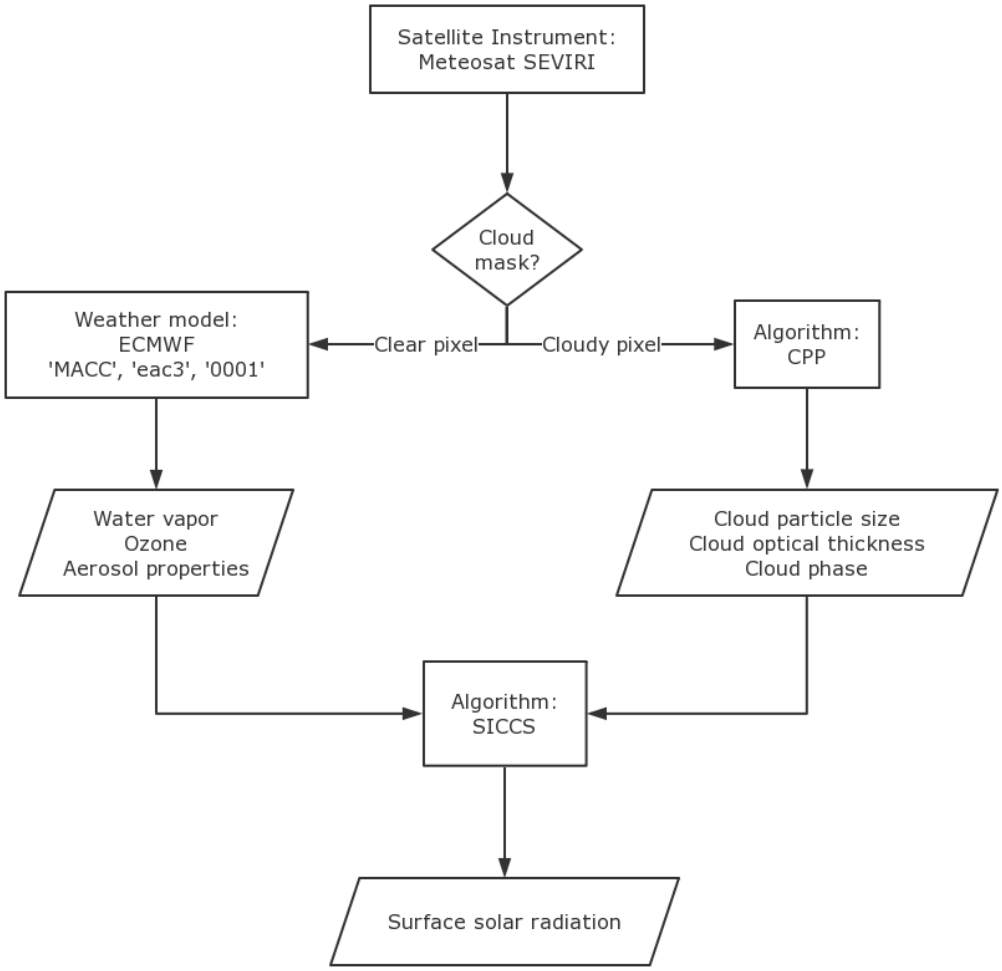

Figure 1.1: *The schematic diagram of CPP-SICCS. SEVIRI: the Spinning Enhanced visible and InfraRed Imager; ECMWF: the European Centre for Medium-Range Weather Forecasts; CPP: Cloud physical properties; SICCS: Surface Insolation under Clear and Cloudy skies derived from SEVIRI imagery.*

1.3 Knowledge gap

Among many of the ongoing research in RDSW, aerosol datasets derived from various sources have been used as the input of SICCS algorithm. The results can be compared or analysed at the same level only if the aerosol datasets were proved to have a great consistency with each other.

CPP-SICCS operated at KNMI has been updated in multiple aspects including the cloud mask procedure, CPP, SICCS, etc., and the recent retrievals include aerosol datasets from '0001' and 'eac3' respectively. The many changes lead to complex impacts on the CPP-SICCS performance. Since many studies were made based on the old CPP-SICCS, to determine if the results are reliable in current context, the difference in two CPP-SICCS versions needs to be confirmed.

According to previous results from satellite observations retrieved by CPP-SICCS, the SDS over shallow waters (coast, lake, etc.) is somehow lower than that on land. This phenomenon has not been well understood yet, and will be investigated later.

1.4 Objective and research questions

The aim of this internship project is to investigate satellite observations and solar radiation from Meteosat SEVIRI and relevant algorithms, as well as the aerosol properties used as input.

To achieve the goal, following research questions need to be answered:

1. What is the consistency among aerosol property datasets '0001', 'eac3' and 'MACC'? And what is the impact caused by their differences?

2. What are the differences between the new and old version of the CPP-SICCS product?

3. What causes lower retrieved SDS over shallow waters compared to lands?

A case study of the IJsselmeer area is performed to answer question 3. Ground-based observations are used here in addition.

1.5 Outline

The study proceeds in three stages, namely the comparison between aerosol property datasets, the comparison between new and old satellite observation algorithm, and a case study about IJsselmeer area. The remainder of this report is organized as follows. In Chapter 2, methodology used in the study is explained including the background of each stage, introduction of datasets and algorithms, data attributes and processing methods. The results and corresponding discussions are presented in the later Chapter 3, 4 and 5 respectively. General discussion and reflection on the deficiencies during the process of research is presented in Chapter 6. Finally Chapter 7 concludes the internship project and offers advices for future work.

Chapter 2 Methodology

In this chapter, the general methodology and procedures used in each part are explained. All data used in this project were provided by KNMI.

2.1 Inter-comparison of aerosol property datasets

The inter-comparison of aerosol property datasets was carried out in two parts, which are the direct comparison of aerosol property datasets, and the comparison of clear sky surface downwelling solar irradiance (SDS_{cs}) with different aerosol datasets as inputs.

2.1.1 Comparison of aerosol property datasets

For the current SDS retrieval ('old SICCS version') the aerosol input is taken from 'MACC' at a fixed year (2008). In the new SICCS version a combination of 'eac3' and '0001' data will be used. Then it is important to determine difference between these datasets. The main aerosol properties studied in this chapter is the aerosol optical thickness at wavelength of 500 nm (AOT_{500}) and the Ångström exponent (A_{exp}), which are provided as output fields from the MACC/CAMS simulations. AOT is a measure of the aerosol load (e.g., urban haze, smoke particles, desert dust, sea salt) distributed within a column of air from the Earth's surface to the top of the atmosphere [22]. AOT reflects the degree to which aerosols prevent the transmission of light by absorption or scattering of light [23]. A_{exp} is the parameter that expresses the spectral dependence of aerosol optical thickness on the wavelength of incident light, which is related to the particle size; the larger the exponent, the smaller the particle size is [24].

Data attributes

Both '0001' and 'eac3' dataset of 2014-2015 have the same resolution. The temporal resolution is 3 hour, which covers 0, 3, 6, 9, 12, 15, 18, 21:00 each day. And the spatial resolution is 0.5 degree in both latitude and longitude. 'MACC' reanalysis of year 2008 was also included. Although the data is from a different year, the variation tendency can be comparable to '0001' and 'eac3'. It has the same spatial resolution as '0001' and 'eac3' do, however, the data is only available at 12:00 each day. All three datasets are retrieved on global scale.

Data analysis

In order to discover general patterns from the large amount of aerosol property data, several analysis and visualization techniques were used in this study, which are contour mapping, difference mapping, histogram, and statistical processing. Comparison study was carried out on global scale, and then narrowed down to European area (range: [30°W, 50°E], [30°N, 70°N]).

2.1.2 Effect of different aerosol properties inputs on clear sky solar radiation using MSG-CPP algorithm

With the existence of clouds, the effects of aerosols, water vapor and ozone on solar radiation are overshadowed. Thus, aerosol is taken into consideration only when it is clear skies. To figure out the direct impact of aerosol on MSG-CPP algorithm, all aerosol property data should be included in SICCS calculation by assuming that every pixel is clear sky. In this way, the influence of clouds is avoided. And the clear sky surface downwelling solar radiation (SDS_{cs}) comes out as the most interesting output in this section.

Data attributes

The aerosol property data at 12:00 from 2nd to 31st July, 2014 from '0001', 'eac3' and 'MACC' (2008) were implemented to MSG-CPP as inputs. The SDS_{cs} output was retrieved from MSG-CPP in KNMI. Since the retrieval relies on solar backscattered radiation, the MSG-CPP only provides products during daytime. The full disk area with valid solar radiation data is in range of [82°W, 81°E] and [82°S, 81°N].

Data analysis

The procedures of data processing and visualization are similar to those in Section 2.1.2.

2.2 Comparison between new and old version of CPP-SICCS product

The comparison between new and old CPP-SICCS was made upon SICCS output, namely surface downwelling solar radiation (SDS), only the cloud effects were taken into account this time. Thus the study also involves comparison of cloud phase identification.

2.2.1 Data attributes

The data is available at 12:00 from 2nd to 31st July, 2014. The full disk area is in range of [82°W, 81°E] and [82°S, 81°N] which depends on MSG satellite observations. In the old version, 'MACC' is the aerosol input, and 'eac3' reanalysis is used in the new version.

2.2.2 Data analysis

The processing methods are similar to previous study, however the data needs to be categorized according to different cloud phases. In the process of cloud mask identification, pixels are divided into three categories which are clear, liquid cloudy, and ice cloudy phases. Based on different cloud phases, the CPP-SICCS calculates SDS with various inputs in various routes (see Figure 1.1). The difference in cloud mask identification has a great influence on SDS derivation. Therefore the agreement of cloud mask performance between two versions is another important thing to look at. The study is also carried out on MSG full disk scale and European scale.

2.3 Case study: Investigation on a special case of IJsselmeer area

In the final part, a case study of IJsselmeer lake area focusing on both satellite observations and ground-based measurements is performed.

The satellite observations show that the SDS over IJsselmeer lake is lower than that over the surrounding lands (see Figure 2.1(a) and Figure 2.1(b)). To achieve a better understanding of this result, which might be an artifact of the retrieval algorithm, detailed research in terms of SDS and cloud phase was applied.

2.3.1 Data attributes

For data in IJsselmeer area, there are 2 sources of information are available, which are satellite observations retrieved by CPP-SICCS and ground-based measurements of several stations.

There are 2 types of satellite observations. One is available at 12:00 from 2nd to 31st July, 2014 in area of [2°E, 7°E] and [50°N, 55°N]. It gives more informations about the atmospheric composition in terms of SDS, cloud phase, cloud physical properties, etc. The other one is aggregated hourly data from 8th September, 2015 to 7th September, 2016 in area of [0°E, 11°E] and [47°N, 57°N].

The KNMI operated network contains three stations around the IJsselmeer: Berkhout, Stavoren and Lelystad. For the period 8th September, 2015 to 7th September, 2016, additional SDS observation were carried out at Houtribdijk. The temporal interval of Houtribdijk is 12 s, and the rest is 10 min. The locations of stations are shown in Figure 2.2. A simulation at Houtribdijk station with temporal interval of 5 min was made by SICCS. It provides simulated SDS_{cs} under clear skies as a reference.

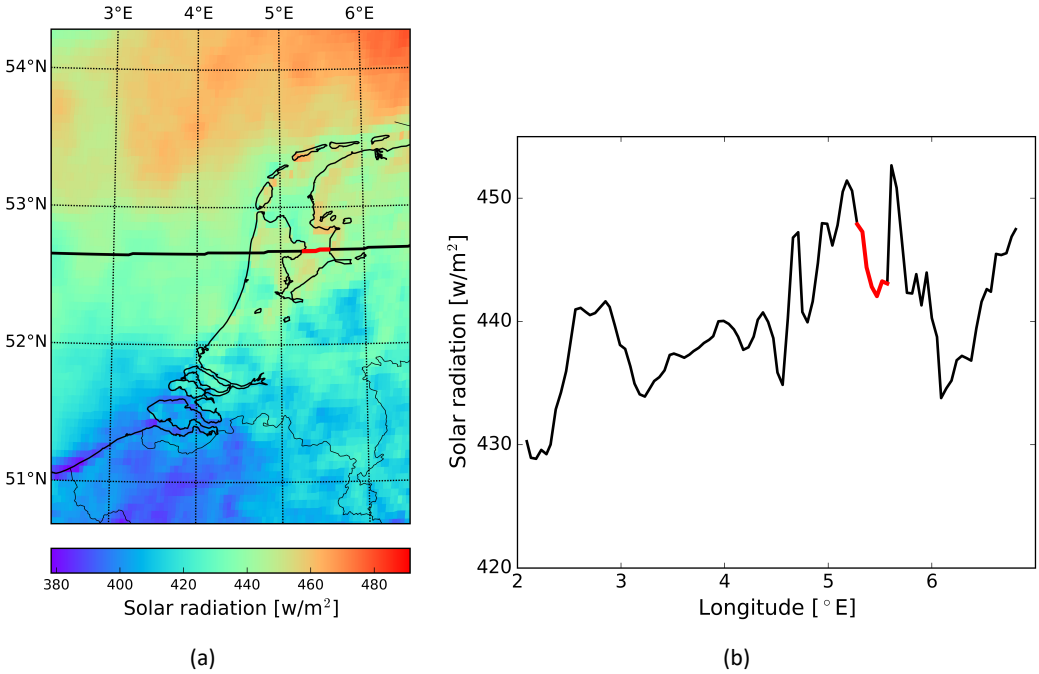

Figure 2.1: *Monthly averaged SDS in 2014/07 retrieved by CPP-SICCS (a) in a contour map of IJsselmeer, (b) on the cross-section at latitude of 52° N. The red line represents SDS data over IJsselmeer lake.*

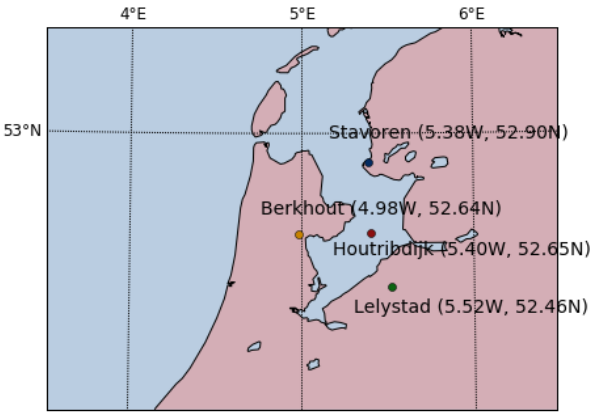

Figure 2.2: *The locations of ground stations around IJsselmeer lake, namely, Houtribdijk, Berkhout, Stavoren and Lelystad. Land and water area are filled with pink and blue colour, respectively.*

2.3.2 Data processing & analysis

The case study was carried out in 4 steps, which are analysis of SDS and cloud phase retrieved from CPP-SICCS, comparison among ground measurements, comparison among the aggregated satellite data, comparison between ground measurements and the aggregated satellite data.

CPP-SICCS satellite observations

In Figure 2.1(a) and Figure 2.1(b), the satellite observations of July, 2014 retrieved by CPP-SICCS shows lower SDS over lake than that over land. As explained earlier, different cloud phases leads to variation in SDS calculation. Thus, in order to understand the result, it is crucial to investigate cloud phases distribution and the corresponding SDS.

Ground-based measurements

The second stage focuses on ground-based measurements. The four stations are located as in Figure 2.2. Houtribdijk station sits in the middle of IJsselmeer lake and is surrounded by other three stations on land. The comparison between Houtribdijk and other stations should be able to provide SDS data to verify the results from satellite observations. However, the solar panel that provides power to Houtribdijk station causes extra light reflection on the meter (see Figure 2.3).

Figure 2.3: *Ground measurement meter on Houtribdijk. A solar panel is placed vertically above the meter.*

In order to obtain credible SDS data from Houtribdijk, the affected data have to be eliminated first. Since no extra information is available besides SDS measurement for Houtribdijk station, a simulated SDS under clear sky is produced by SICCS as a reference to help identify the problematic data. The processed Houtribdijk measurement is plotted against data from Berkhout, Stavoren and Lelystad respectively in scatter plots.

Aggregated satellite observations

The next part is to compare the aggregated hourly satellite data at the four ground stations. The same comparison scatter plots between Houtribdijk and other station are made.

Ground measurements versus aggregated satellite observations

After comparing SDS above water with SDS on land of both ground and satellite observations, the last step is to verify the agreement between these two methods. Since the temporal intervals of ground and satellite data are different, firstly the ground measurement data are integrated to 1 h which is consistent to the aggregated satellite data. Then the scatter plots between satellite and ground measurements of each station are made.

Chapter 3 Results & discussions on inter-comparison of aerosol datasets

The results of inter-comparison of aerosol property datasets are presented in two parts, which are direct comparison of aerosol properties, and comparison of clear sky solar radiation with different aerosol properties as inputs.

3.1 Comparison of aerosol property datasets

3.1.1 Global Area

The contour mappings of AOT_{500} and A_{exp} in January and July, 2014 provided by '0001' are shown in Figure 3.1 and 3.2. Generally speaking, AOT_{500} on the northern hemisphere is higher in July than that in January, and the opposite situation is applied to southern hemisphere. Several main peaks appear in eastern China, India and central Africa in both months, which can be explained by that these large developing economy bodies lead to more industrial emissions and biomass burning. In July, a high AOT_{500} in Sahara is caused by serious desert dust in dry season. And some unusual high numbers occur in Canada and Russia in 2014/07 which are caused by forest fires.

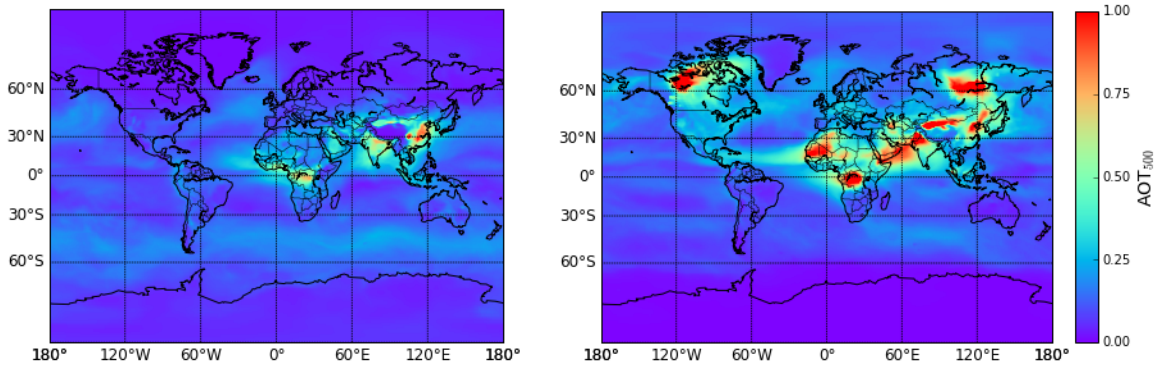

(a) (b)

Figure 3.1: *Contour mapping of averaged AOT_{500} in (a) 2014/01 and (b) 2014/07 from '0001' dataset in global area.*

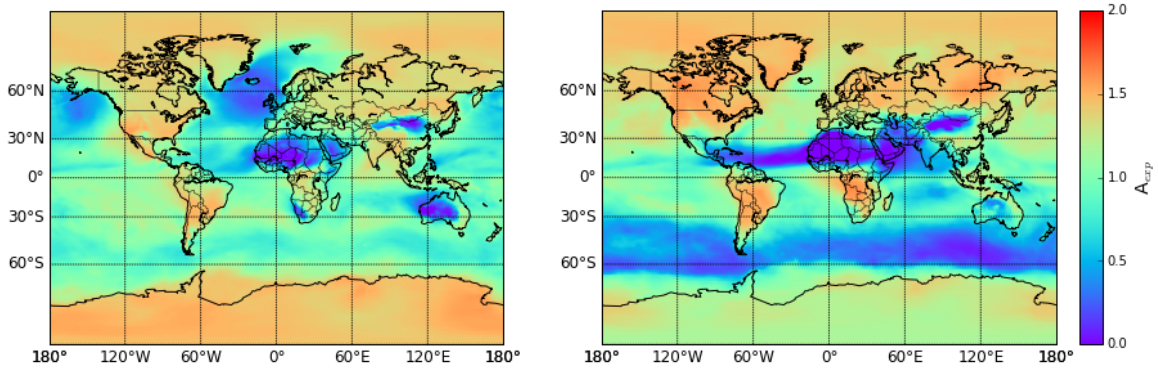

(a) (b)

Figure 3.2: *Contour mapping of averaged A_{exp} in (a) 2014/01 and (b) 2014/07 from '0001' in global area.*

A_{exp} does not show a distinct seasonal pattern in the Northern Hemisphere, although in the Southern Hemisphere A_{exp} reduces from January to July. In particular, very low A_{exp} is observed in desert region (Sahara, Taklamakan, Gobi, Australia, etc.) related to the relative large size of desert dust particles. In contrast, industrial activity and biomass burning generate smaller particles (higher A_{exp}).

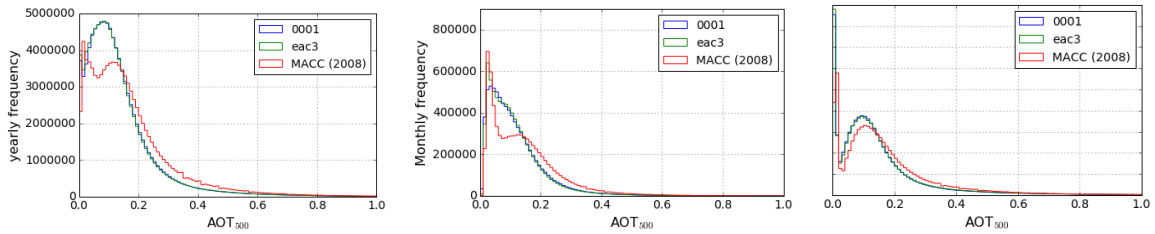

(a) (b) (c)

Figure 3.3: *Histograms of AOT_{500} in (a) year 2014, (b) 2014/01 and (c) 2014/07 from '0001', 'eac3' and 'MACC' in global area. 'MACC' data is of the same month in year 2008. 100 bins are applied. Frequency refers to the number of pixels attributed to one bin.*

Histograms of AOT_{500} and A_{exp} are presented in Figure 3.3 and 3.4. As presented in the Figure 3.3(a), the frequency distributions of AOT_{500} in '0001' and 'eac3' are almost identical over year 2014, and 'MACC' of 2008 deviates from others. The difference between '0001'/'eac3' are mostly related to the very different model configuration that produced these datasets. To a smaller extent the different year of 'MACC' data might also play a role. In addition, the 'MACC' has a smaller sample size than CAMS data do. As mentioned in Section 2.1.2, the temporal resolution of '0001' and 'eac3' is 3 hour, while 'MACC' is only available for 12:00 each day.

A major peak appears around AOT_{500} close to 0 in July. It seems to be that there are large areas with very little aerosols in the atmosphere where can be confirmed as south pole combined with the AOT_{500} contour mapping Figure 3.1(b). However, it is noted that the frequencies in two poles have been exaggerated, because the same amount of grid cells are located in a smaller surface area. A large amount of data fall in between AOT_{500} of 0 to 0.1. In July more pixels have higher AOT_{500} than in January. Extremely high AOT_{500} occurs in more polluted/populated areas such as eastern China, India and mid-Africa.

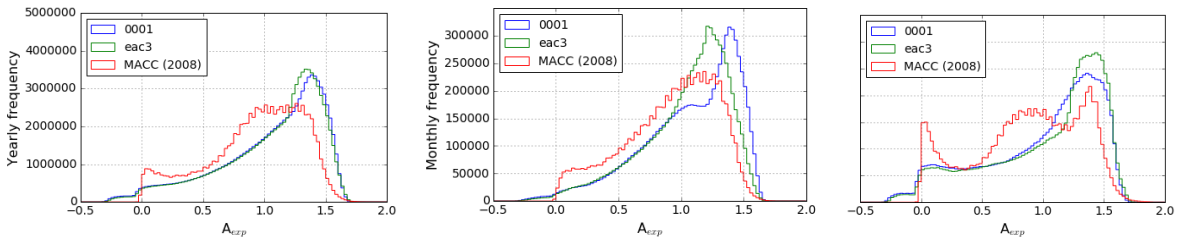

(a) (b) (c)

Figure 3.4: *Histograms of A_{exp} in (a) year 2014, (b) 2014/01 and (c) 2014/07 from '0001', 'eac3' and 'MACC' in global area. 'MACC' data is of the same month in year 2008. 100 bins are applied.*

Yearly speaking, the distribution of A_{exp} (Figure 3.4(a)) in '0001' is quite comparable to that in 'eac3', while 'MACC' curve shows larger difference compared to AOT_{500} histogram. 'MACC' has very few negative A_{exp} values which mostly happen during dust events. In range of A_{exp} from 0 to 1.2, 'MACC' has higher frequencies over '0001' and 'eac3'; it has less amount in higher A_{exp}.

It can be observed from Figure 3.4(b) and Figure 3.4(c) that lower A_{exp} values are in July and higher A_{exp} are in January, which means larger aerosols occur in July and smaller aerosols are in January. The increasing desert dust events in July are responsible for the larger aerosols, and the smaller aerosols in

January could be caused by biomass burning for heating purposes in January.

It is shown in Figure 3.5 that the means of '0001' matches those of 'eac3' very well. Both AOT_{500} and A_{exp} have seasonal patterns. The averaged AOT_{500} is higher in July than in January. The means of 'MACC' from 2008 is higher than '0001'/'eac3' from either 2014 or 2015. A_{exp} from June to August are slightly lower than those in other time period. The means of 'MACC' are about 0.2 lower than '0001' and 'eac3'.

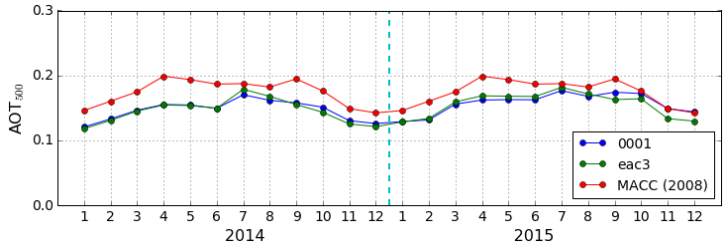

(a)

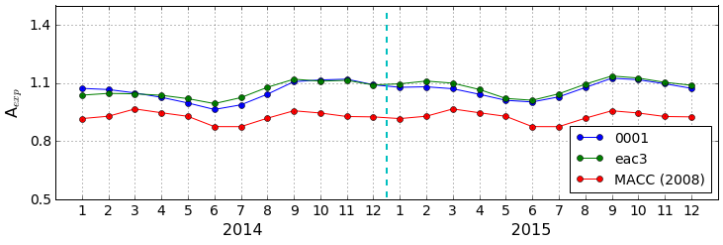

(b)

Figure 3.5: *Monthly means of (a) AOT_{500} and (b) A_{exp} from '0001', 'eac3' and 'MACC' in global area. '0001' and 'eac3' data are in sequence of 2014 and 2015. 'MACC' curve is repeated data of 2008.*

3.1.2 European Area

The data located in European region were processed into monthly and yearly histograms in the same way as global data were, and the results are shown in Figure 3.6 and 3.7. Yearly speaking, AOT_{500} in '0001' and 'eac3' have very similar distributions; compared to that, 'MACC' has less distribution in AOT_{500} range [0, 0.2], but more in higher AOT_{500}. For three datasets, the frequencies of AOT_{500} have similar distribution in both January and July, except that the peaks move to right side, and become less steep in July. It means more light transmission was prevented in July.

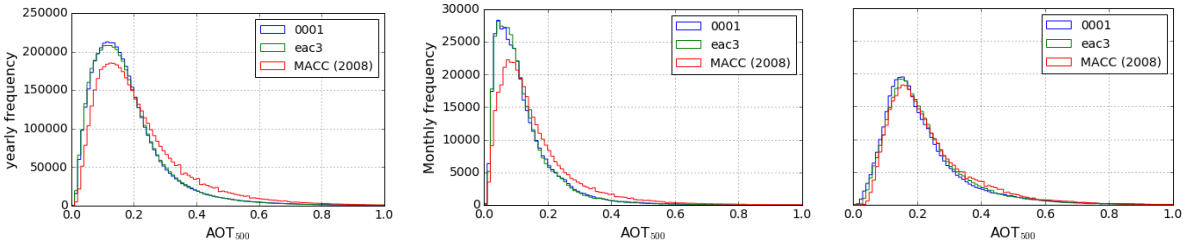

(a) (b) (c)

Figure 3.6: *Histograms of AOT_{500} in (a) year 2014, (b) 2014/01 and (c) 2014/07 from '0001', 'eac3' and 'MACC' in European area. 'MACC' data is of the same month in year 2008. 100 bins are applied.*

'0001' and 'eac3' have very comparable pattern in A_{exp} distribution. A_{exp} frequency curves have distinct seasonal changes. All three datasets present a bipolar shape in January, of which the large number of low A_{exp} is due to the large-sized particles above the ocean (Figure 3.2(a)). In July, a steep peak is located around A_{exp} of 1.4.

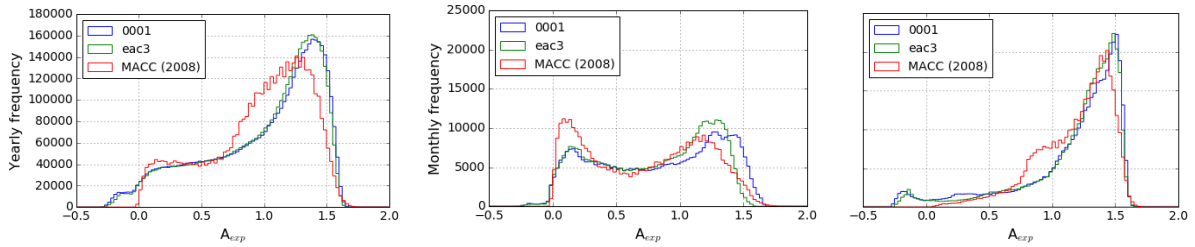

(a) (b) (c)

Figure 3.7: *Histograms of A_{exp} from '0001', 'eac3' and 'MACC' in European area for (a) year 2014, (b) 2014/01 and (c) 2014/07. 'MACC' data is of the same month in year 2008. 100 bins are applied.*

As shown in Figure 3.8, the tendencies present seasonal changes. It can be conducted that in European area, the amount of atmospheric particles is larger in July, but the size becomes smaller compared to January. The similarity of means between '0001' and 'eac3' data is very high. For AOT_{500}, 'MACC' is higher than '0001'/'eac3'. A_{exp} of 'MACC' has a little fluctuations from '0001' and 'eac3'.

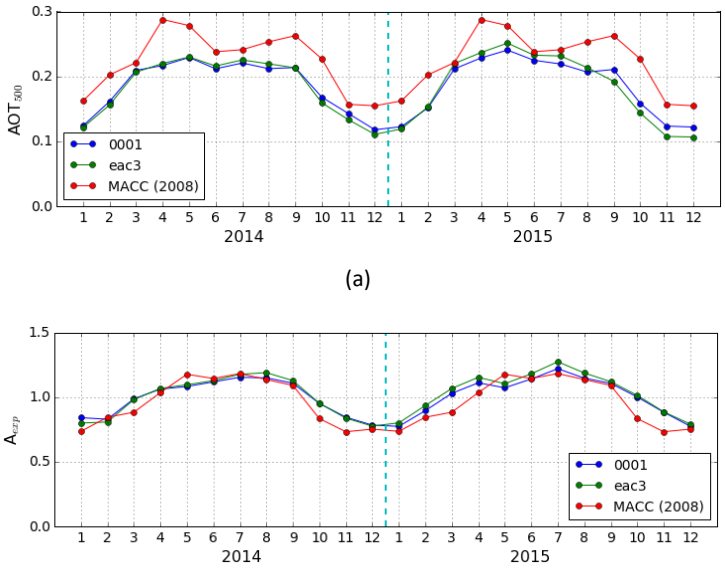

(a)

(b)

Figure 3.8: *Monthly means of (a) AOT_{500} and (b) A_{exp} from '0001', 'eac3' and 'MACC' in European area. 'MACC' curve is repeated data of 2008.*

Table 3.1 summarize the yearly mean values of AOT_{500} and A_{exp} for both European and global region. The difference of mean AOT_{500} values between '0001' and 'eac3' is less than 0.7 % in both global and European scale. For A_{exp} there are variations of 1.5 % and 0.3 % between '0001' and 'eac3' globally and over Europe respectively. 'MACC' dataset has 20 % higher AOT average compared to '0001'/'eac3', and lower A_{exp} (approximately 14 % globally and 3 % over Europe).

Table 3.1: *Mean values of AOT_{500} and A_{exp} from '0001', 'eac3' and 'MACC' datasets*

	AOT_{500}			A_{exp}		
	'0001' [3]	**'eac3'** [3]	**'MACC'** [4]	**'0001'**	**'eac3'**	**'MACC'**
Global [1]	0.146	0.145	0.174	1.053	1.069	0.925
Europe [2]	0.186	0.185	0.224	0.992	0.995	0.961

[1] global mean of AOT_{500} or A_{exp}
[2] mean of AOT_{500} or A_{exp} in Europe
[3] from datasets in 2014 and 2015
[4] from dataset in 2008

3.2 Effect of different aerosol properties inputs on clear sky solar irradiance using MSG-CPP algorithm

Clear sky downwelling solar irradiance (SDS_{cs}) is the amount of solar radiation reaching the surface without the consideration of cloud effects. It reflects the impact of aerosols on solar radiation. By introducing different aerosol properties derived form '0001', 'eac3' and 'MACC' dataset, MSG-CPP is able to generate the corresponding SDS_{cs} on MSG full disk and European scales.

3.2.1 MSG full disk area

In Figure 3.9, the averaged SDS_{cs} computed by MSG-CPP algorithm with aerosol data from '0001' is plotted in a contour map (Figure 3.9(a)). The differences between '0001'/'eac3' and '0001'/MACC are also presented. SDS_{cs} calculated based on '0001' and 'eac3' have similar results (Figure 3.9(b)). However, it can be observed from Figure 3.9(c) that the SDS_{cs} of 'MACC' in 2008 has larger deviation up to 40 W/m^2 from '0001'. The averaged SDS with 'eac3' and 'MACC' can be found in Figure A.1 and Figure A.2 in Appendix.

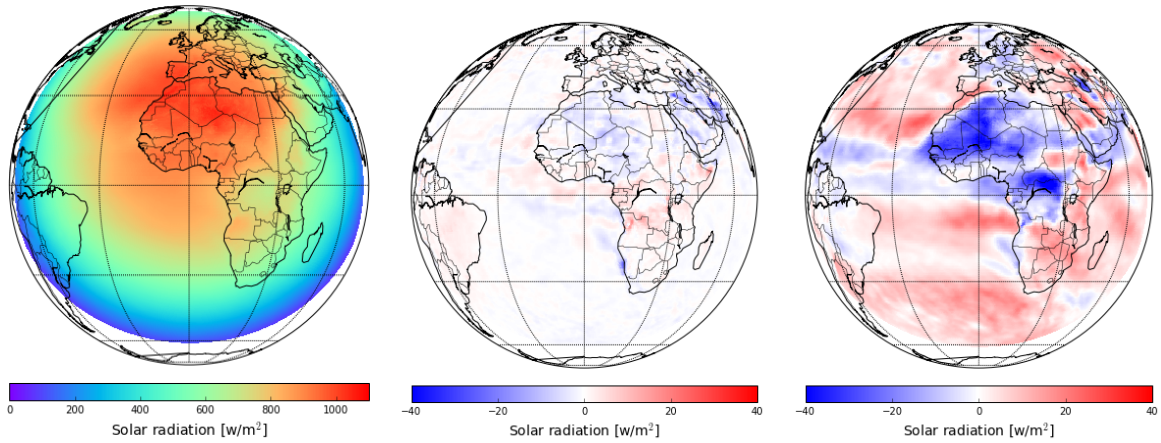

(a) (b) (c)

Figure 3.9: *(a) Contour mapping of averaged SDS_{cs} in 2014/07 retrieved by MSG-CPP using aerosol data from '0001'. Difference mapping of averaged SDS_{cs} between (b) '0001'/'eac3' and (c) '0001'/'MACC' in MSG full disk area. 'MACC' data is of the same month in year 2008.*

The histogram of SDS_{cs} over July was plotted in Figure 3.10. The frequency distributions of '0001' and 'eac3' are highly matched. 'MACC' has slightly lower frequencies in peak range around 850 W/m^2, and a little more around 1000 W/m^2.

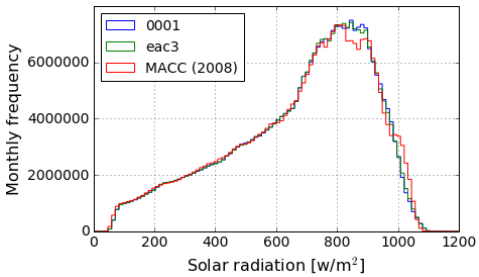

Figure 3.10: *Histogram of* SDS_{cs} *in 2014/07 retrieved by MSG-CPP using aerosol data from '0001', 'eac3' and 'MACC' in MSG full disk area. 'MACC' data is of the same period in year 2008. 100 bins are applied.*

The daily means of SDS_{cs} in full disk calculated over July were plotted in time series (Figure 3.11). The curves of '0001' and 'eac3' are almost identical. 'MACC' has the similar pattern but is slightly lower than '0001'/'eac3'.

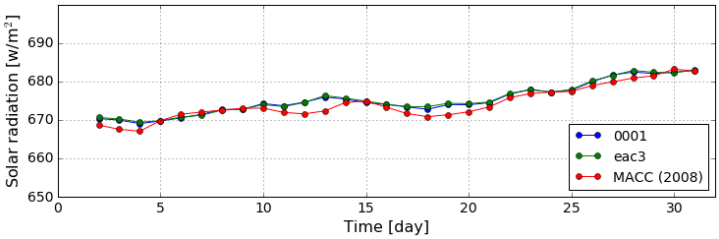

Figure 3.11: *Daily means of* SDS_{cs} *retrieved by MSG-CPP using aerosol data from '0001', 'eac3' and 'MACC' in MSG full disk area. '0001' and 'eac3' data are from 2014/07. 'MACC' data is of the same month in year 2008.*

3.2.2 European Area

SDS_{cs} calculated with '0001' and 'eac3' aerosol data have very similar frequency distributions, while 'MACC' has a larger distribution around SDS_{cs} of 900 W/m^2 (Figure 3.12).

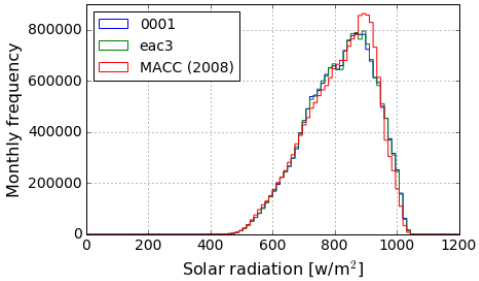

Figure 3.12: *Histogram of* SDS_{cs} *in 2014/07 retrieved by MSG-CPP using aerosol data from '0001', 'eac3' and 'MACC' in European area. 'MACC' data is of the same month in year 2008. 100 bins are applied.*

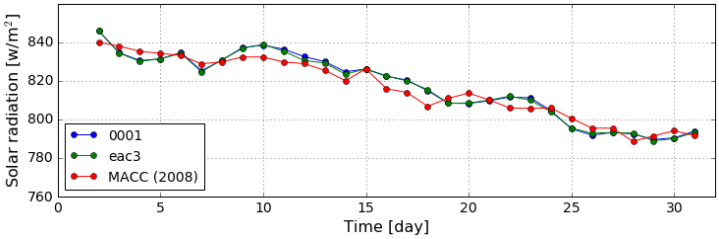

Figure 3.13: *Daily means of* SDS_{cs} *retrieved by MSG-CPP using aerosol data from '0001', 'eac3' and 'MACC' in European area. '0001' and 'eac3' data are from 2014/07. 'MACC' data is of the same month in year 2008.*

As shown in Figure 3.13, '0001' and 'eac3' curves overlap almost completely, and 'MACC' only has small deviations from the other two.

Table 3.2: *Mean values of* SDS_{cs} *[W/m^2] in July retrieved by MSG-CPP using aerosol data from '0001', 'eac3' and 'MACC'.*

	'0001' [3]	**'eac3'** [3]	**'MACC'** [4]
full disk [1]	675.24	675.38	674.21
Europe [2]	817.09	816.87	815.90

[1] mean of SDS_{cs} in full disk
[2] mean of SDS_{cs} in Europe
[3] using datasets in 2014
[4] using dataset in 2008

In Table 3.2 the monthly mean SDS_{cs} with three datasets are presented. Using aerosol property data from the three different sources, which are '0001', 'eac3' and 'MACC', only leads to a slight difference (less than 0.2 %) on the outcome of MSG-CPP algorithm. Note that the AOT difference between 'eac3'/'0001' and 'MACC' was relatively small for July 2014 (Figure 3.8(a)), so for other months somewhat larger differences in SDS_{cs} may be expected.

To sum up, the aerosol properties which are AOT_{500} and A_{exp} from '0001' and 'eac3' reanalysis in 2014 and 2015 are very close in both global and European scale; 'MACC' dataset from 2008 has small deviations from '0001' and 'eac3'. Moreover, using '0001', 'eac3' or 'MACC' as input in MSG-CPP algorithm delivers similar results. Slightly lower SDS in 'MACC' is consistent with higher AOT_{500} in combination with lower A_{exp}.

Chapter 4 Results & discussions on CPP-SICCS algorithm

In this chapter, the outcomes of new and old version of CPP-SICCS are compared on both MSG full disk and European scale. For this comparison all 12:00 UTC SEVIRI images in July 2014 are used.

4.1 MSG full disk area

Figure 4.1(a) and Figure 4.1(b) show the averaged SDS retrieved from new CPP-SICCS and the difference between the new and old in the full disk area. It can be observed that the new version has been improved to expand the observation boundary. The two versions deliver close results. The average map of old version is in Figure A.3 in Appendix.

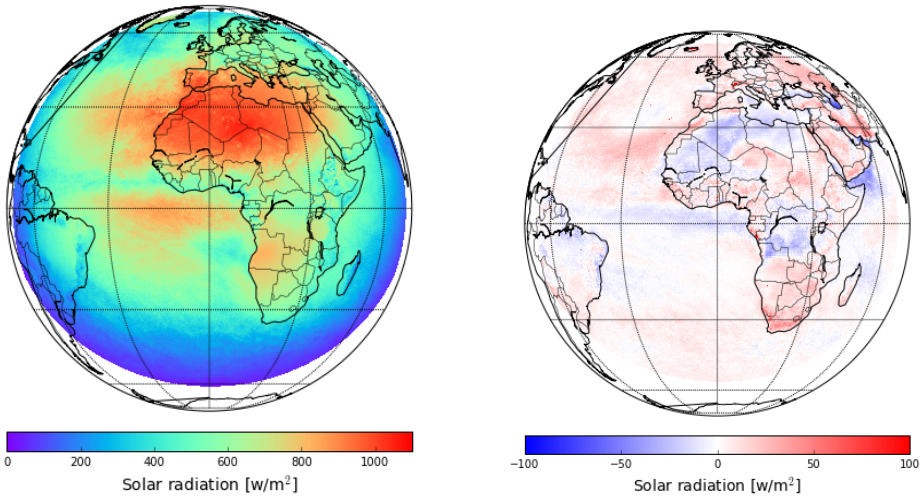

Figure 4.1: *(a) Contour mapping of averaged* SDS *in 2014/07 retrieved by new CPP-SICCS. (b) Difference mapping of averaged* SDS *retrieved by new and old CPP-SICCS in MSG full disk area.*

4.1.1 9 scenarios by cloud phase identification

Pixels from new and old CPP-SICCS are categorized by three different cloud phases respectively. Since the cloud mask system was modified, cloud phase of the same pixel in two versions can be differeng, which leads to 9 scenarios of cloud phases as listed in Table 4.1. The biggest proportions are taken by scenarios where cloud phase is identified as clear or liquid cloudy by both new and old versions. The agreement in cloud phase identification between the two versions reaches 79.61 %.

The data over 2014/07 have been collected to form the histograms (Figure 4.2), and the results of 9 scenarios are presented in the same layout as Table 4.1. It can be observed from the plots with consistent identification that, strong solar radiation mostly happens in clear skies, and the strength decreases as the sky becomes cloudy. The same pattern applies to all histograms in old version. In most of the histograms, curves of new and old versions match well. Only the plot at left bottom corner shows larger deviation which can be accounted for the smaller sample size.

Note that some peaks around SDS of 0 appear in the ice cloudy scenarios of the old version. These are caused by an empirical SDS correction in the old version.

Table 4.1: *Percentage of 9 scenarios of cloud phase distribution in 2014/07 retrieved by new and old CPP-SICCS in MSG full disk area.*

		New version		
		clear	**liquid cloudy**	**ice cloudy**
Old version	**clear**	36.09 % [1]	6.47 %	1.29 %
	liquid cloudy	5.11 %	35.20 %	5.92 %
	ice cloudy	0.08 %	1.53 %	8.32 %

[1] 'Percentage' refers to the ratio between number of pixels attributed to each scenario and total number of pixels.

Figure 4.2: *Histograms of SDS in 2014/07 retrieved by new and old CPP-SICCS in 9 scenarios in MSG full disk area.*

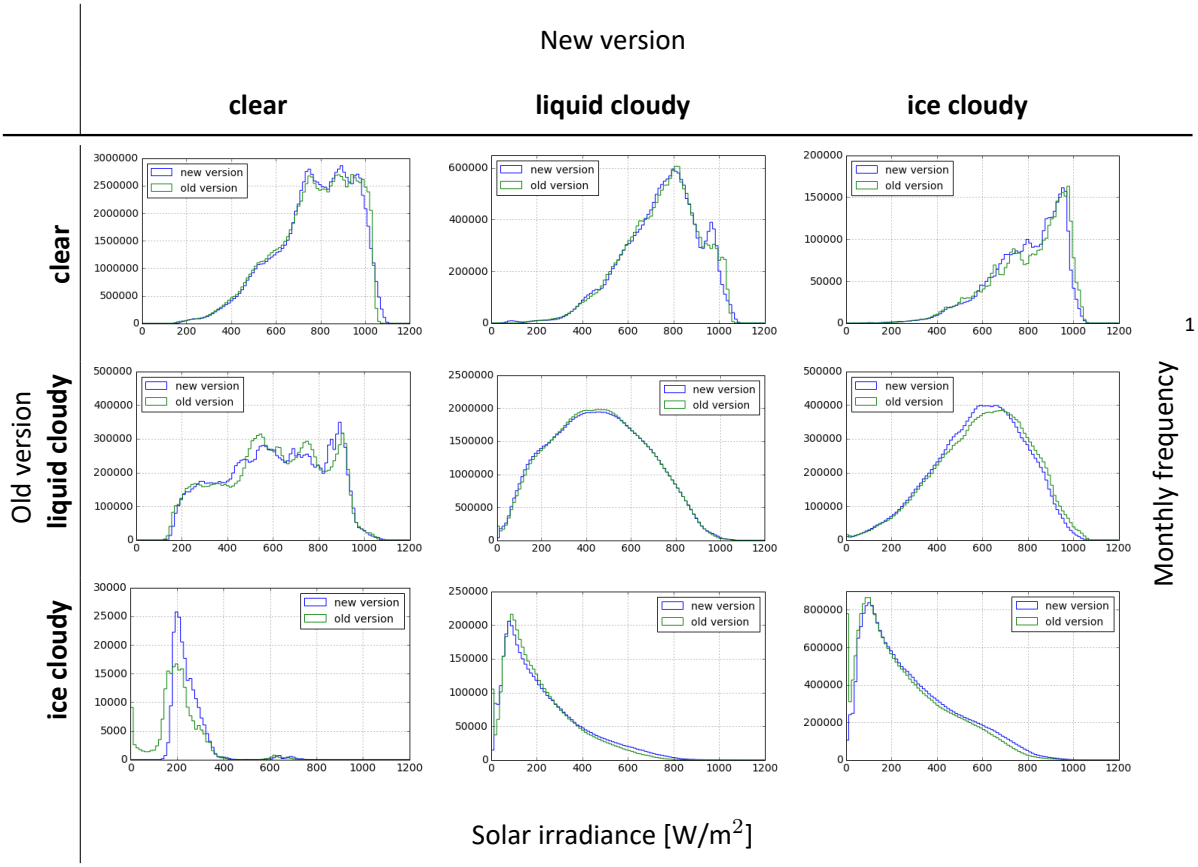

[1] 100 bins are applied to histograms.

4.1.2 Statistical analysis

The mean SDS of new and old version in terms of each scenario are calculated (Table 4.2) . The relative differences ($\frac{\overline{new}-\overline{old}}{\overline{old}} \times 100\%$) are within ± 3 % except for ice cloud scenarios in the old version which is caused by the empirical correction as outlined before.

Table 4.2: *Monthly statistics of* SDS *in 2014/07 retrieved by new and old CPP-SICCS in 9 scenarios in MSG full disk area.*

		New version			
		clear	**liquid cloudy**	**ice cloudy**	Parameter
Old version	**clear**	775.58	745.38	791.58	$\overline{new}$ [W/m^2] [1]
		771.52	747.62	800.75	$\overline{old}$ [W/m^2] [2]
		0.53	-0.30	-1.15	$\frac{\overline{new}-\overline{old}}{\overline{old}} \times 100$ [%]
	liquid cloudy	605.53	460.00	588.99	$\overline{new}$ [W/m^2]
		599.57	461.42	604.72	$\overline{old}$ [W/m^2]
		0.99	-0.31	-2.60	$\frac{\overline{new}-\overline{old}}{\overline{old}} \times 100$ [%]
	ice cloudy	246.83	233.98	288.05	$\overline{new}$ [W/m^2]
		205.67	213.76	259.56	$\overline{old}$ [W/m^2]
		20.01	9.46	10.98	$\frac{\overline{new}-\overline{old}}{\overline{old}} \times 100$ [%]

[1] monthly mean of SDS retrieved by new CPP-SICCS.
[2] monthly mean of SDS retrieved by old CPP-SICCS.

4.2 European area

4.2.1 9 scenarios by cloud phase identification

The percentages of pixels in different cloud phase scenarios within the European area are shown in Table 4.3 . The consistency of cloud phase distributions between new and old CPP-SICCS is 79.06 % which is close to the result in full disk case. However, less liquid cloudy and more ice cloudy pixels are found in the European area.

The impact of cloud mask identification on SDS calculation can be conducted from some plots in Figure 4.3 . For instance, when the sky is identified as liquid cloudy in old version but clear sky in new, the curve of the new version shifts to right from the old. It is because SDS is calculated higher under the clear sky state than in cloudy sky.

4.2.2 Statistical analysis

Statistics of SDS in European area are listed in Table 4.4 . Neglecting the ice cloudy scenarios in old version, the relative differences of mean SDS ($\frac{\overline{new}-\overline{old}}{\overline{old}} \times 100$ %) are in range of ± 4 % which is 1 % higher than that in full disk scale but still small.

By comparing new and old CPP-SICCS products in terms of cloud mask identification and SDS, it can

Table 4.3: *Percentage of 9 scenarios of cloud phase distribution in 2014/07 by new and old CPP-SICCS in European area.*

		New version		
		clear	**liquid cloudy**	**ice cloudy**
Old version	**clear**	35.90 %	3.75 %	1.19 %
	liquid cloudy	5.29 %	27.87 %	8.01 %
	ice cloudy	0.00	2.69 %	15.29 %

Figure 4.3: *Histograms of SDS in 2014/07 retrieved by new and old CPP-SICCS in 9 scenarios in European area.*

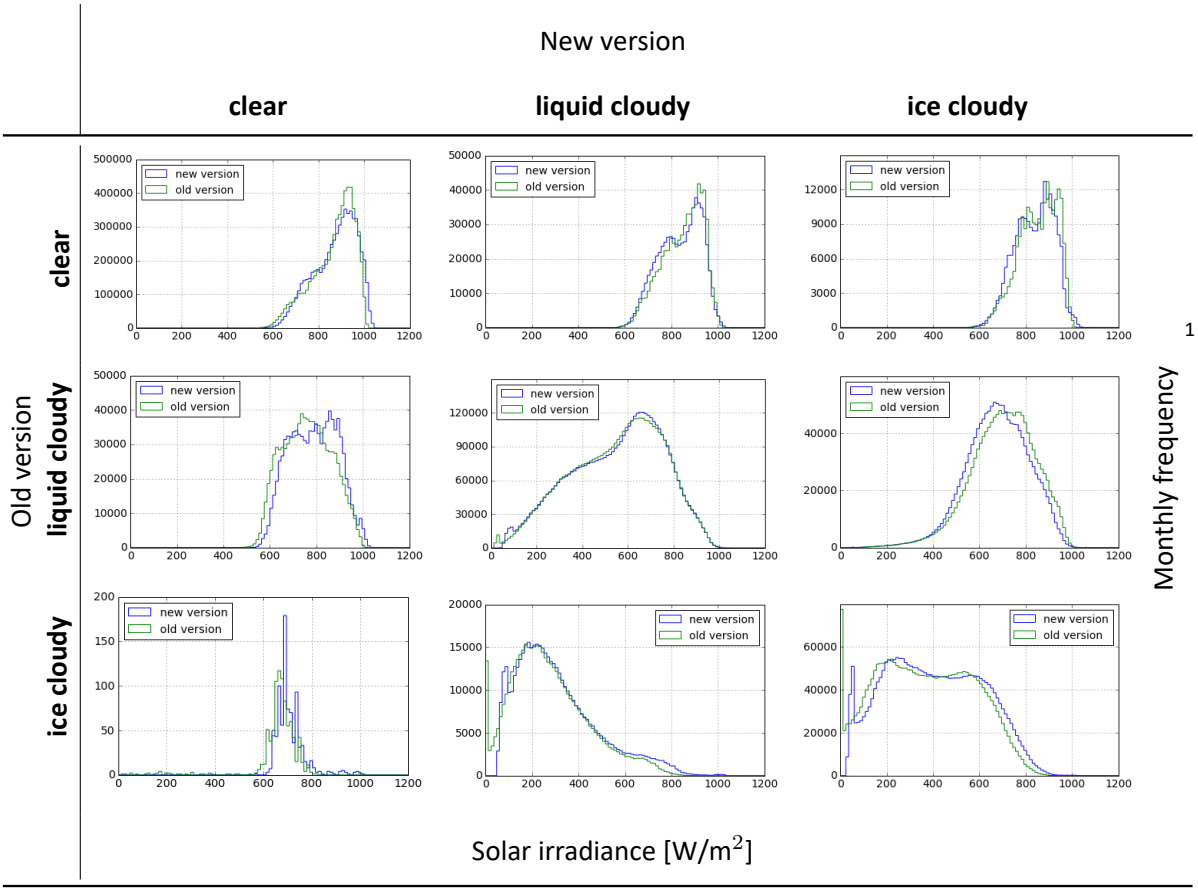

[1] 100 bins are applied to histograms.

Table 4.4: *Monthly statistics of SDS in 2014/07 retrieved by new and old CPP-SICCS in 9 scenarios in European area.*

		New version			
		clear	**liquid cloudy**	**ice cloudy**	Parameter
Old version	**clear**	873.13	836.69	836.75	$\overline{new}$ [W/m^2] [1]
		866.25	848.71	851.20	$\overline{old}$ [W/m^2] [2]
		0.79	-1.42	-1.70	$\frac{\overline{new}-\overline{old}}{\overline{old}} \times 100$ [%]
	liquid cloudy	788.18	553.08	676.42	$\overline{new}$ [W/m^2]
		760.68	551.94	700.80	$\overline{old}$ [W/m^2]
		3.62	0.21	-3.48	$\frac{\overline{new}-\overline{old}}{\overline{old}} \times 100$ [%]
	ice cloudy	710.97	308.74	403.75	$\overline{new}$ [W/m^2]
		660.97	278.27	368.91	$\overline{old}$ [W/m^2]
		7.56	10.95	9.44	$\frac{\overline{new}-\overline{old}}{\overline{old}} \times 100$ [%]

[1] monthly mean of SDS retrieved by new CPP-SICCS.
[2] monthly mean of SDS retrieved by old CPP-SICCS.

be concluded that even though around 20 % difference exists in cloud phase identification, the final outcome SDS is not much affected except for cases identified as ice cloudy by the old version, because the old CPP-SICCS contains an empirical correction of the ice cloud transitivity.

Chapter 5 Results & discussion on case study in IJsselmeer area

5.1 CPP-SICCS satellite observations

As shown in Figure 2.1(a), the monthly surface solar radiation over IJsselmeer lake is lower than that of surrounding land area, and the cross section at latitude of 52°N (Figure 2.1(b)) has further proved a reduction of SDS over water area. Data from 2014/07 at latitude of 52°N were collected and studied in terms of cumulative SDS and cloud phase (CPH).

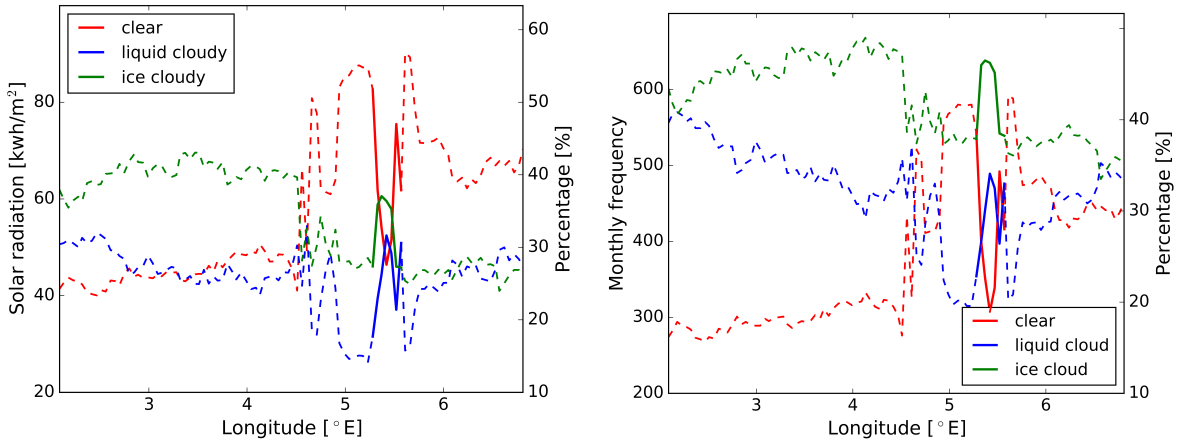

Figure 5.1: *SDS and CPH at latitude of 52°N in 2014/07 retrieved by CPP-SICCS. (a) Cumulative SDS energy (kWh/m^2) and its percentage under different skies, (b) Monthly CPH frequency and its percentage. Frequency refers to the amount of pixels attributed to one cloud phase category. The solid lines represent the data over IJsselmeer lake area.*

The curve in Figure 2.1(b) is decomposed into 3 parts (Figure 5.1(a)) when the cloud phase is identified as clear, liquid cloudy and ice cloudy respectively. Apparently, SDS under clear skies has a significant decrease from land to lake area, meanwhile SDS under cloudy skies increases. The frequencies of occurrence of three cloud states are shown in Figure 5.1(b). Over the lake area, the percentage of clear pixels decreases by 20 %.

It can be concluded that the lower SDS from satellite observation over IJsselmeer lake area is caused mainly by the reduced clear sky identification.

5.2 Ground Measurements

5.2.1 Elimination of problematic data of Houtribdijk measurements

To eliminate the problematic data suffering from solar panel reflection, SICCS simulation with the assumption of fully clear sky is employed as reference. Some examples are presented in Figure 5.2.

In one of the clear sky cases (Figure 5.2(d)), there is an unusual bump around noon hours which is apparently caused by solar panel reflection. However in a cloudy sky case from a nearby date (Figure 5.2(e)), it is difficult to identify which part is affected. Thus the approach is to find out the pattern in fully clear sky days, and apply it to all sky.

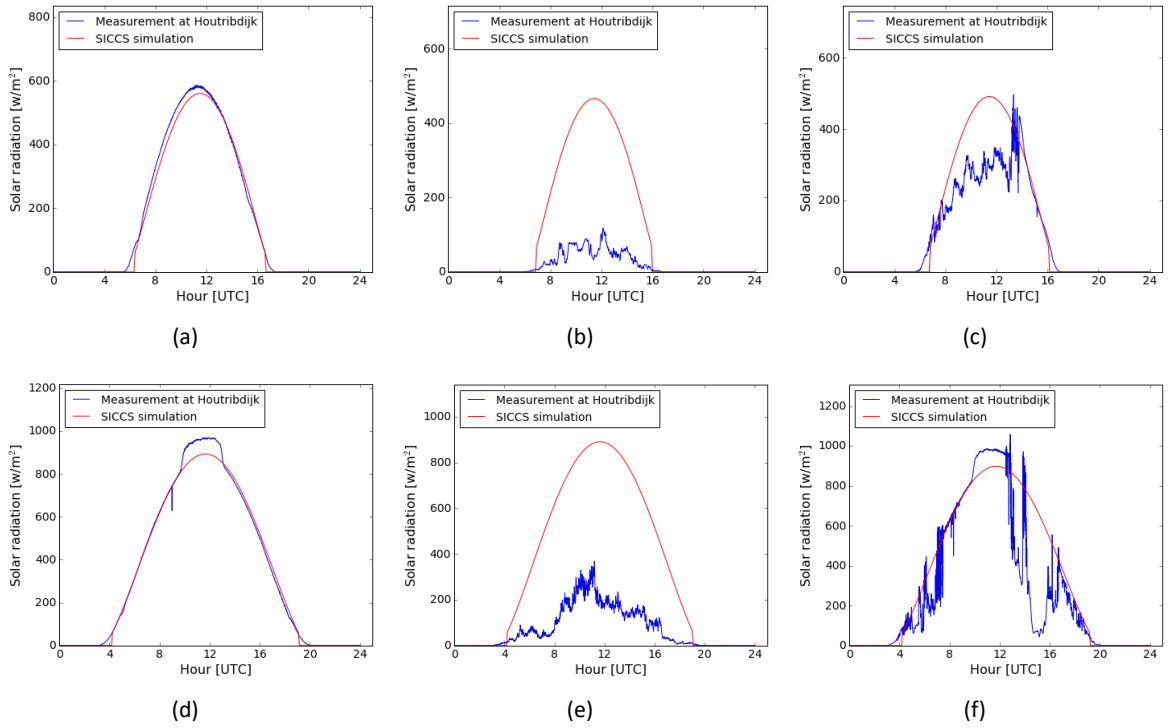

Figure 5.2: *SDS measurements at Houtribdijk station on (a) fully clear sky: 2015/10/01, (b) heavily cloudy sky: 2015/10/16, (c) mixed: 2015/10/12, (d) fully clear sky: 2016/06/05, (e) heavily cloudy sky: 2016/06/02 and (f) mixed: 2016/06/22. Blue lines represent ground measurement, and red lines represent simulated SDS by SICCS at the same place.*

The reflection effect is very likely to vary by seasonal change. The clear sky curve from another season in Figure 5.2(a) does not show abnormality. This means the reflection increases as solar elevation angle increases. Therefore to find out which time period in a day and which days in a year are affected by the reflection are the main goals of this part.

To exclude biases in simulation, firstly a simple correction was made to fit the SICCS simulation to the part of measurements that are not affected. To translate it into mathematical language, it is to minimize the quadratic function shown as eq. (5.1),

$$\sum_{i=1}^{N} (SDS_{m,i} - \alpha\, SDS_{siccs,i})^2 \tag{5.1}$$

where $SDS_{m,i}$ and $SDS_{siccs,i}$ are SDS of measurement and SICCS simulation at time i respectively, α is the correction factor, and N is the final time.

Then a search for points i where $(SDS_{m,i} - \alpha\, SDS_{siccs,i}) = 0$ is performed to calculate when the reflection starts and ends, and the corresponding time points are denoted as t_0 and t_f.

The next step is to determine the amount of reflected energy SDS_{rfl} (J/m^2) by integrating the solar radiation between time t_0 and t_f (eq. (5.2)). An inequality constraint (eq. (5.3)) is applied to i to guarantee the integration taking place in a continuous interval.

$$SDS_{rfl} = \int_{t_0}^{t_f} (SDS_{m,i} - SDS_{siccs,i}) \tag{5.2}$$

subject to

$$8.34 \leq i \leq 14.33 \tag{5.3}$$

Fully clear sky days are selected for investigation. The start and end time of reflection effect and the amount of reflected energy are listed in Figure 5.3.

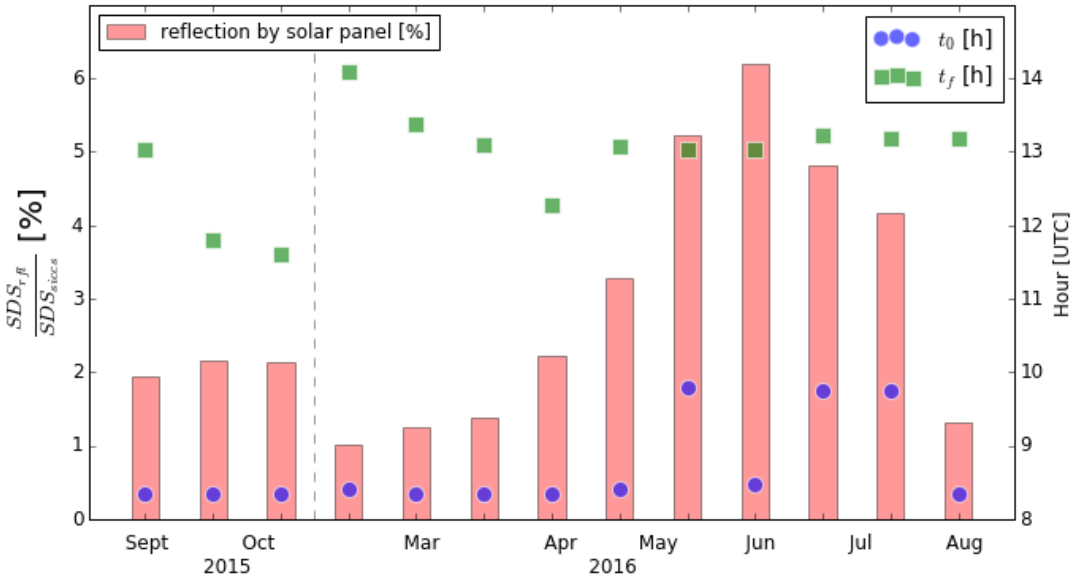

Figure 5.3: *Problematic data profile of SDS measurements at Houtribdijk station. Each bin represents a fully clear day. Pink bars associated with the left y-axis represent* $\frac{SDS_{rfl}}{SDS_{siccs}} \times 100$ *%. Purple circles and green squares corresponding to the right y-axis represent* t_0 *and* t_f *respectively.*

As shown in Figure 5.3, started from September 2015, the percentage of reflection ($\frac{SDS_{rfl}}{SDS_{siccs}}$) stays low (under 3 %) until May 2016, then it increases to the peak on 6th of July, and falls back to low level in August. Thus the mostly influenced months are May, June and July, and most of the affected hours are pretty close.

It is decided that the data elimination only takes place in the range between the last day of low $\frac{SDS_{rfl}}{SDS_{siccs}}$ before May and the first day of low $\frac{SDS_{rfl}}{SDS_{siccs}}$ after July. Also the eliminated data should cover most of the affected hours, which is 9:30 - 13:30 in period 2016/04/12 - 2016/08/17 for all sky. In order to have a fair comparison with other station measurements, data in the same time slots have been removed from other station measurements as well.

5.2.2 Comparison among ground measurements

The plots of SDS measurements from four ground stations can be found in Figure A.4, Appendix. For fully clear sky days, every station except Houtribdijk has comparable or slightly lower SDS than SICCS simulation does. It proves that the SICCS simulation result is reliable.

Beside the fully clear and the heavily cloudy days, there are more days mixed with clear and cloudy hours. For better use of these valuable samples, the data of clear and cloudy skies need to be separated. For this purpose, a simple cloud phase identification system was raised.

The principle is shown in Figure 5.4. SDS under 50 W/m^2 usually appears at dawn or evening when the sunlight is too weak to identify the cloud phase. Thus SDS under 50 W/m^2 is excluded from cloud phase classification. SICCS simulation is used as a reference. When SDS is larger than 90 % of SICCS simulation, and maintains continuous for at least 30 min, this part is identified as clear sky. In contrary, if SDS is lower than 70 % of SICCS simulation, it is categorized as cloudy sky.

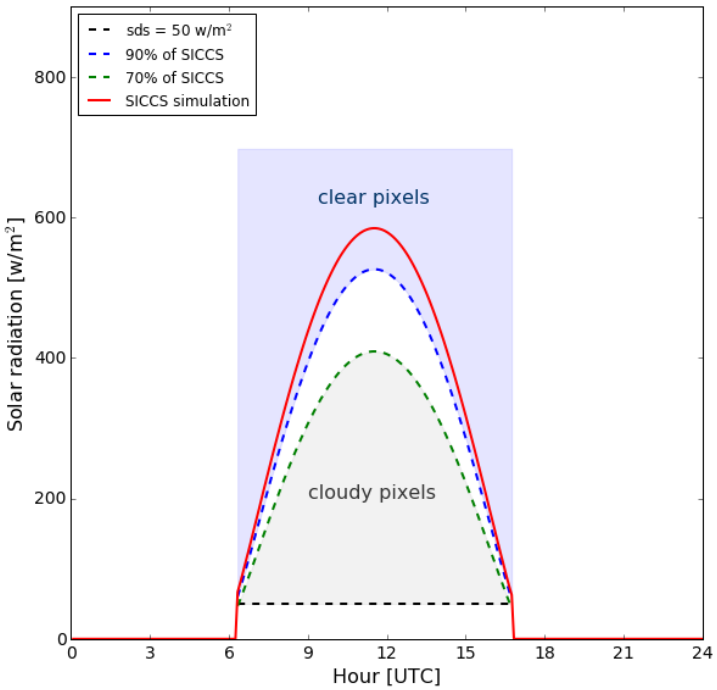

Figure 5.4: *Cloud phase identification system.*

With cloud phase classification, comparison scatter plots between Houtribdijk measurements and other stations provide further information. As shown in Figure 5.5, measurements of Houtribdijk and Berkhout stations from the same time are scattered against each other. The linear fit is produced by ordinary least square linear regression. Station Stavoren and Lelystad deliver similar results which can be found in Figure A.5 in Appendix.

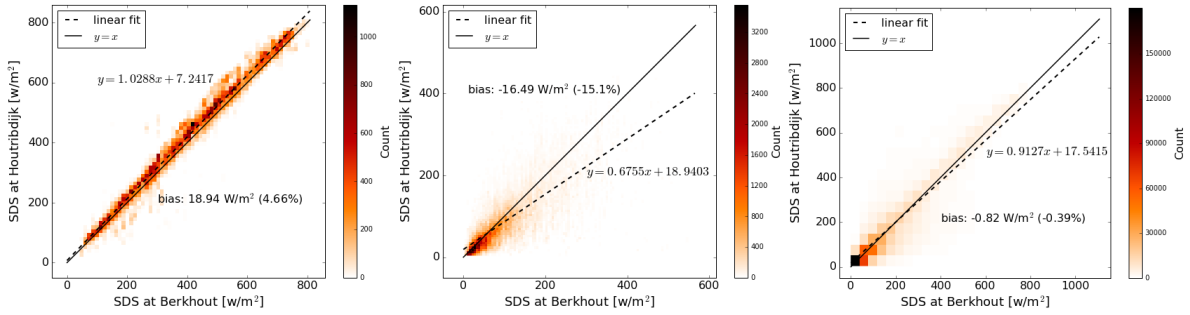

(a) (b) (c)

Figure 5.5: *Comparison scatter plots between ground measurements of Houtribdijk and Berkhout stations under (a) clear sky, (b) cloudy sky and (c) all sky in the period 2015/09/08 - 2016/09/07. X- and Y- values of each point represent SDS measurements of Berkhout and Houtribdijk at the same time. Quantities of square bins in each plot are 60, 100 and 23 respectively. Colours reflect the occurrence frequency in each bin. Black solid line represents* $y = x$*, and dash line represents the linear fit produced by ordinary least square regression.*

For clear sky cases, the slopes of linear fits are all above 1, which means Houtribdijk has higher measurements than other station do. The opposite results are found in cloudy hours. Houtribdijk measurements are about 15 % lower than other stations on land. With all measurements together, the result is in between clear and cloudy cases, but still Houtribdijk has lower radiation measurement in general.

The lower radiation measurements of Houtribdijk in cloudy hours respond to the results found in satellite observation. However, the higher measurements in clear hours implies that the extra radiation by solar

panel reflection still remains influential in clear skies after data elimination. And it is highly possible that the affected time period exceeds the previous estimation.

5.3 Aggregated satellite observations

The retrieved satellite observations from CPP-SICCS was aggregated into hourly data.

The SDS data falling at each station spot are extracted in time series. The cloud phase identification system described in Figure 5.4 is also applied to separate clear and cloudy pixels. And then the comparison between Houtribdijk station and other stations are performed in scatter plots (Figure 5.6 and Figure A.6 in Appendix).

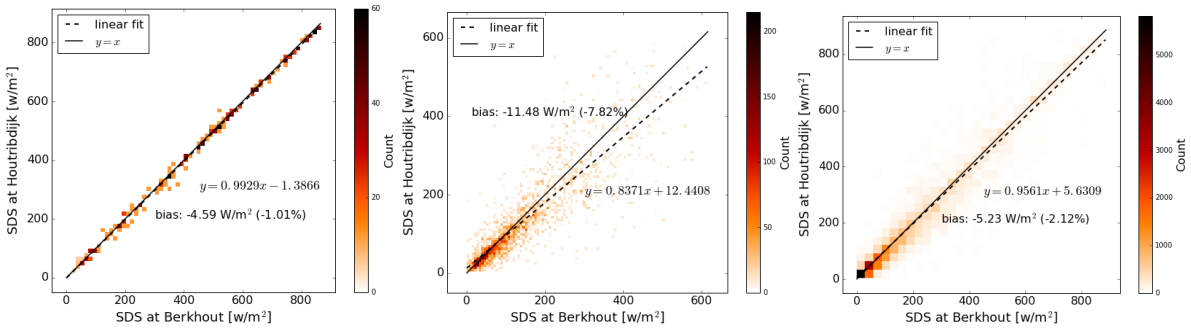

Figure 5.6: *Comparison scatter plots between satellite observations of Houtribdijk and Berkhout stations retrieved from CPP-SICCS under (a) clear sky, (b) cloudy sky and (c) all sky in period 2015/09/08 - 2016/09/07. Quantities of square bins in each plot are 60, 100 and 30 respectively.*

It can be observed from Figure 5.6 that, SDS at Houtribdijk is generally 1 - 2 % lower than other stations. For clear sky cases, Houtribdijk only has 1 % lower measurements, although about 8 % difference is found in cloudy pixels.

5.4 Ground measurements versus satellite observations

The results for all sky cases gained from ground measurements and satellite observations do not have a perfect agreement. One reason could be that the problematic data elimination in ground measurements leads to incomplete data sample. In order to test the agreement between the two methods, data of the same time slots is taken out from the aggregated CPP-SICCS satellite observations. And the comparison scatters are presented in Figure 5.7 .

The agreements between satellite observations and ground measurements are pretty good in general. For clear sky, all stations deliver similar result that the satellite measurements are lower than ground measurements. Houtribdijk has the largest negative bias which means ground measurement is overestimated more compared to other stations. This can be related to the extra reflection on Houtribdijk's meter. Under cloudy sky, similar results that lower satellite data are found compared to ground-based data can be found in four stations. Regardless cloud phases, satellite observation is higher than ground measurement at Berkout, Stavoren and Lelystad. For Houtribdijk, the overestimation of ground measurement under clear sky balances out the underestimation under cloudy sky and it results in the smallest bias of all stations.

The scatters of clear sky at Berkhout, Stavoren and Lelystad are quite dispersed compared to Houtribdijk. It is possible that some cloudy pixels are mixed within it. One of the reason could be an estimation made during cloud phase separation. When MSG SEVIRI taking an image of the Earth, there are time delays from place to place. As explained in Figure 5.4, the cloud phase separation proceeds based on the

Figure 5.7: *Comparison scatter plots between satellite observations and ground measurements at each ground stations (Houtribdijk, Berkhout, Stavoren and Lelystad) under clear sky, cloudy sky and all sky in period 2015/09/08 - 2016/09/07. 40 square bins are applied in all scatter plots.*

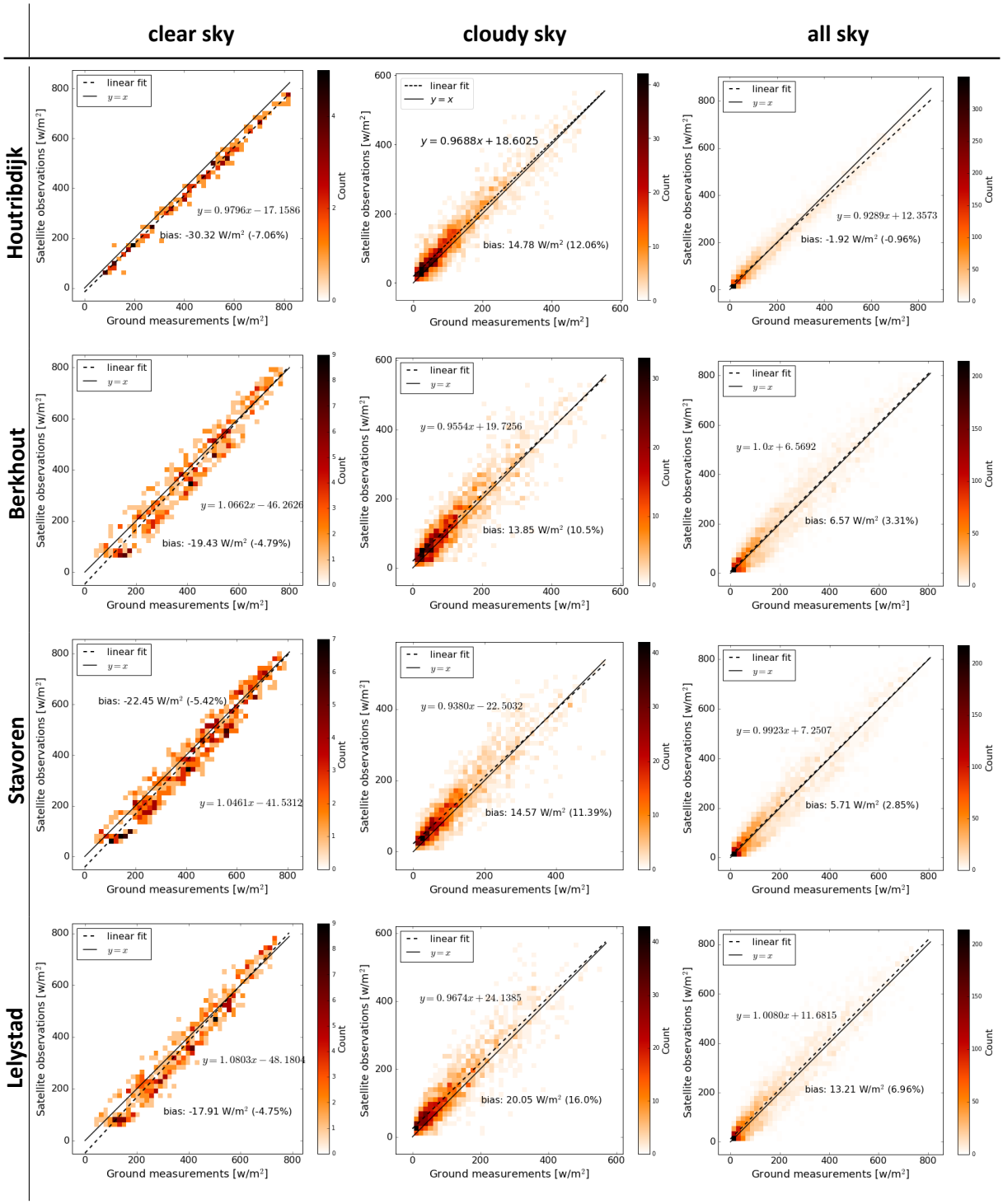

SICCS simulation at Houtribdijk, which means measurements at Berkhout, Stavoren and Lelystad were categorized according to the simulation at Houtribdijk. This rough estimation introduced extra noises.

The case study reveals that more retrieved clouds over IJsselmeer lake surface leads to the lower SDS, and the Houtribdijk ground measurements cannot be trusted. Furthermore, CPP-SICCS satellite data and other ground station measurements have a good agreement in general.

Chapter 6 General discussion

During the project, comparison studies were performed on multiple subjects. Although reasonable results were delivered, there were still some factors affecting accuracy of the study.

The most common problem is the difference in data resolution/interval. As mentioned in Chapter 2, some data in comparison have various time intervals due to the fact that they are usually retrieved from different sources or calculated by different algorithms. In this case, data have to be integrated or interpolated in order to adapt each other. The rough estimations and inappropriate processing methods introduced error.

In some cases the sample size is not large enough to obtain credible results. For example in Figure 4.2 , the scenario with ice cloudy in old version and clear in new version has a very small sample size compared to other scenarios. It is difficult to determine if a general pattern can be revealed from current results.

The type of satellite projection brought biases in a statistical point of view. Figure 3.1 and 3.2 presents a Miller projection with gridded data in a square shape. However in reality, earth is a sphere and the surface area varies with latitude. The consequences of expanding a sphere surface to a square is that the influences of data on two poles have been greatly exaggerated than the data on equator.

Besides the problem existing in data themselves, the more significant issue is inadequate data processing method, especially for IJsselmeer study. Due to the lack of knowledge on data/image recognition, some complicated problems were prejudged subjectively or manually. For instance, the fully clear sky and heavily cloudy days in Figure 5.2 were selected manually; and the cloud phase identification criterion depicted in Figure 5.4 was simplified to a linear relation which is regarded as a reasonable assumption. Regarding Houtribdijk measurements, the data elimination did not result in a credible result, even though some efforts have been made to recognize the problematic data. These simple processing and rough estimations led to some information loss.

As a reflection on the internship project, several lessons can be learned. First, pre-processing of data is important. Before actual analysis, it is necessary to fix any faulty parts in raw data and unify their resolutions and units. Second, doubtful results have to be specified and excluded from further analysis. At last, subjective judgements need to be avoided and more machine-based processing methods can be helpful.

Chapter 7 Conclusion

The study was performed in three parts which are inter-comparison of aerosol datasets, comparison of CPP-SICCS algorithms, and a case study on IJsselmeer area.

Three aerosol datasets, '0001' (2014 & 2015), 'eac3' (2014 & 2015) and 'MACC' (2008), used in KNMI research have very similar AOT_{500} and A_{exp} on both global and European scale. And using them as inputs in MSG-CPP algorithm results in similar clear-sky surface radiation (SDS_{cs}). Thus including either of the aerosol datasets in SDS calculation will not introduce large variations.

By comparing the performance of new and old CPP-SICCS products in 2014/07, it is found that around 20% difference exists in cloud phase identification process, but still the SDS shows high consistency. Overall the two versions have a good agreement.

The case study on IJsselmeer reveals that more clouds are retrieved over the lake area which causes the lower SDS than the surrounding lands. Measurements at Houtribdijk, which were performed to provide ground truth on the surface radiation over the IJsselmeer, turned out to be seriously affected by the solar panel reflection (including but not restricted to period 9:30 - 13:30 in 2016/04/12 - 2015/08/17) and the current processing is not sufficient to convert it into reliable data. CPP-SICCS satellite data and ground measurements at the surrounding land stations, including Berkhout, Stavoren and Lelystad stations, have high consistencies.

Acknowledgements

I would like to express my gratitude to all those who helped me during the internship research.

My deepest gratitude first and foremost goes to my internship supervisor, Dr.Jan Fokke Meirink, for his constant encouragement and patient guidance. This internship would not have been possible without his support.

Second, I would like to thank my colleagues in the Department of R&D Satellite Observations (RDSW), KNMI for supporting me during the work.

Finally I would like to thank dr.Karel Keesman and dr.Ton van Boxtel, Biobased Chemistry & Technology (BCT) group of Wageningen University & Research for providing valuable suggestions and help on internship affairs.

References

[1] IEA, "Key world energy statistics 2016," in *Key world energy statistics 2016*, 2016.

[2] M. Deshmukh and S. Deshmukh, "Modeling of hybrid renewable energy systems," *Renewable and Sustainable Energy Reviews*, vol. 12, no. 1, pp. 235–249, 2008.

[3] M. Deshmukh and S. Deshmukh, "Modeling of hybrid renewable energy systems," *Renewable and Sustainable Energy Reviews*, vol. 12, no. 1, pp. 235–249, 2008.

[4] M. Šúri and J. Hofierka, "A new gis-based solar radiation model and its application to photovoltaic assessments," *Transactions in GIS*, vol. 8, no. 2, pp. 175–190, 2004.

[5] J. Hofierka, M. Suri, *et al.*, "The solar radiation model for open source gis: implementation and applications," in *Proceedings of the Open source GIS-GRASS users conference*, vol. 2002, pp. 51–70, 2002.

[6] W. Greuell, J. Meirink, and P. Wang, "Retrieval and validation of global, direct, and diffuse irradiance derived from seviri satellite observations," *Journal of Geophysical Research: Atmospheres*, vol. 118, no. 5, pp. 2340–2361, 2013.

[7] R. Müller, U. Pfeifroth, C. Träger-Chatterjee, J. Trentmann, and R. Cremer, "Digging the meteosat treasure—3 decades of solar surface radiation," *Remote Sensing*, vol. 7, p. 8067–8101, Jun 2015.

[8] M. Noia, C. Ratto, and R. Festa, "Solar irradiance estimation from geostationary satellite data: I. statistical models," *Solar Energy*, vol. 51, no. 6, pp. 449–456, 1993.

[9] KNMI, "About knmi." `http://www.knmi.nl/over-het-knmi/about`.

[10] KNMI, "R&d satellite observation." `https://www.knmi.nl/research/satellite-observations`.

[11] D. Kim and V. Ramanathan, "Solar radiation budget and radiative forcing due to aerosols and clouds," *Journal of Geophysical Research: Atmospheres*, vol. 113, no. D2, 2008.

[12] V. Ramanathan, P. J. Crutzen, J. Lelieveld, A. P. Mitra, D. Althausen, J. Anderson, M. O. Andreae, W. Cantrell, G. R. Cass, C. E. Chung, A. D. Clarke, J. A. Coakley, W. D. Collins, W. C. Conant, F. Dulac, J. Heintzenberg, A. J. Heymsfield, B. Holben, S. Howell, J. Hudson, A. Jayaraman, J. T. Kiehl, T. N. Krishnamurti, D. Lubin, G. McFarquhar, T. Novakov, J. A. Ogren, I. A. Podgorny, K. Prather, K. Priestley, J. M. Prospero, P. K. Quinn, K. Rajeev, P. Rasch, S. Rupert, R. Sadourny, S. K. Satheesh, G. E. Shaw, P. Sheridan, and F. P. J. Valero, "Indian ocean experiment: An integrated analysis of the climate forcing and effects of the great indo-asian haze," *Journal of Geophysical Research: Atmospheres*, vol. 106, no. D22, pp. 28371–28398, 2001.

[13] Y. J. Kaufman, I. Koren, L. A. Remer, D. Tanré, P. Ginoux, and S. Fan, "Dust transport and deposition observed from the terra-moderate resolution imaging spectroradiometer (modis) spacecraft over the atlantic ocean," *Journal of Geophysical Research: Atmospheres*, vol. 110, no. D10, pp. n/a–n/a, 2005. D10S12.

[14] A. Inness, F. Baier, A. Benedetti, I. Bouarar, S. Chabrillat, H. Clark, C. Clerbaux, P. Coheur, R. Engelen, Q. Errera, *et al.*, "The macc reanalysis: an 8 yr data set of atmospheric composition," *Atmospheric chemistry and physics*, vol. 13, pp. 4073–4109, 2013.

[15] J. Flemming, A. Benedetti, A. Inness, R. J. Engelen, L. Jones, V. Huijnen, S. Remy, M. Parrington, M. Suttie, A. Bozzo, *et al.*, "The cams interim reanalysis of carbon monoxide, ozone and aerosol for

2003–2015," *Atmospheric Chemistry and Physics*, vol. 17, no. 3, pp. 1945–1983, 2017.

[16] CAMS, "Copernicus atmosphere monitoring service." https://atmosphere.copernicus.eu.

[17] EUMETSAT, "Meteosat second generation (msg) provides images of the full earth disc, and data for weather forecasts." https://www.eumetsat.int/website/home/Satellites/CurrentSatellites/Meteosat/index.html.

[18] R. Roebeling, H. Deneke, and A. Feijt, "Validation of cloud liquid water path retrievals from seviri using one year of cloudnet observations," *Journal of applied Meteorology and Climatology*, vol. 47, no. 1, pp. 206–222, 2008.

[19] R. Roebeling, A. Feijt, and P. Stammes, "Cloud property retrievals for climate monitoring: Implications of differences between spinning enhanced visible and infrared imager (seviri) on meteosat-8 and advanced very high resolution radiometer (avhrr) on noaa-17," *Journal of Geophysical Research: Atmospheres*, vol. 111, no. D20, 2006.

[20] P. Stammes, "Spectral radiance modelling in the uv-visible range," in *IRS 2000: Current problems in atmospheric radiation*, pp. 385–388, 2001.

[21] KNMI, "Msg cloud physical properties (cpp)." http://msgcpp.knmi.nl.

[22] NASA, "Aerosol optical depth." https://aeronet.gsfc.nasa.gov/new_web/Documents/Aerosol_Optical_Depth.pdf.

[23] NASA, "Aerosol optical thickness." https://disc.gsfc.nasa.gov/data-holdings/PIP/aerosol_optical_thickness_or_depth.shtml.

[24] NASA, "Angstrom exponent." https://disc.gsfc.nasa.gov/data-holdings/PIP/aerosol_angstrom_exponent.shtml.

Appendix A Supplementary figures

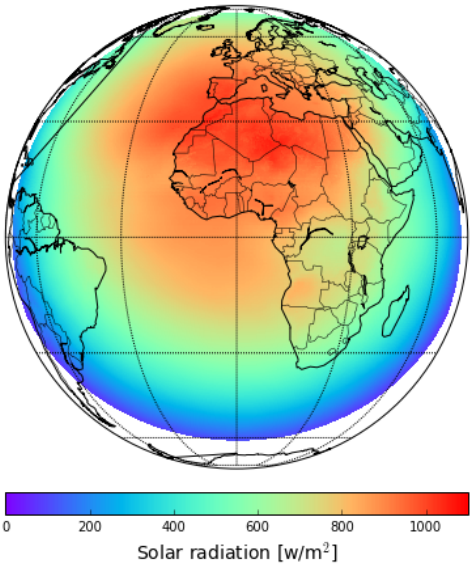

Figure A.1: *Averaged* SDS_{cs} *with 'eac3'*

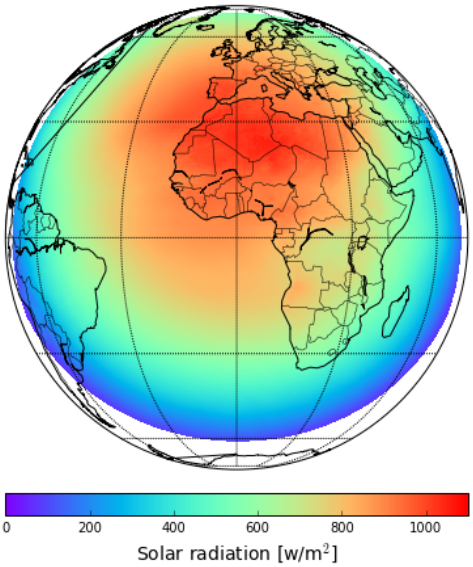

Figure A.2: *Averaged* SDS_{cs} *with 'MACC'*

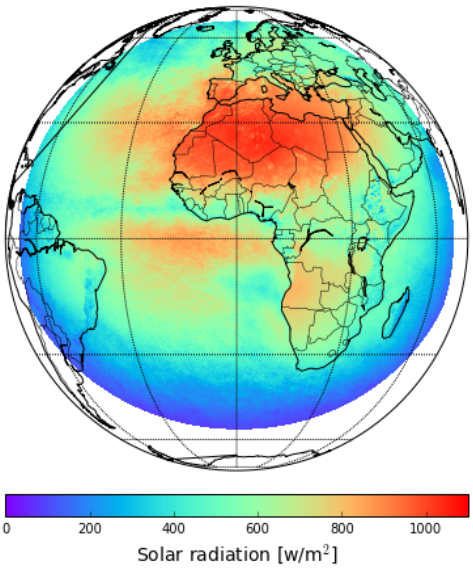

Figure A.3: *Average* SDS *(old CPP-SICCS)*

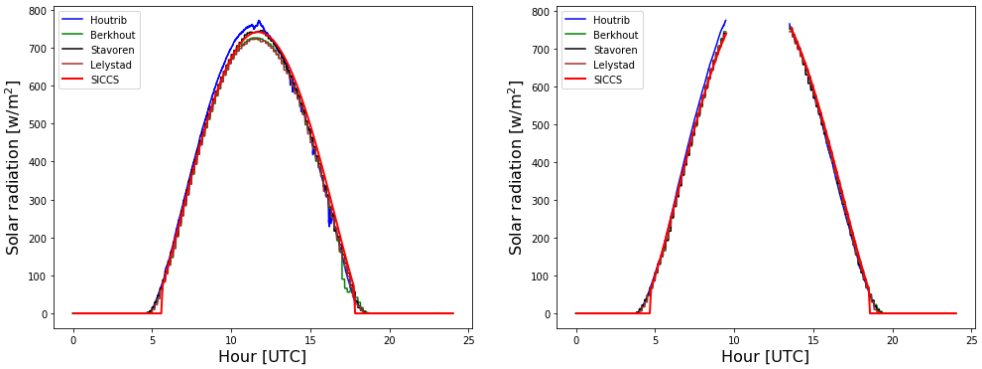

(a) 2016/04/11 (b) 2016/05/08

Figure A.4: *SDS measurements at Houtribdijk, Berkhout, Stavoren and Lelystad on fully clear days.*

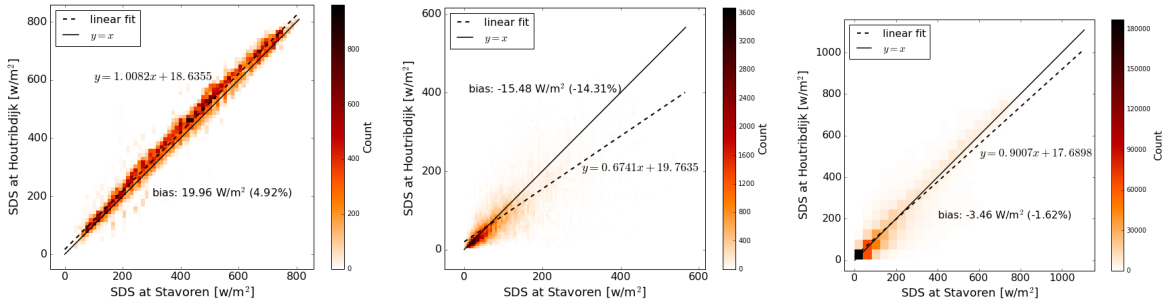

(a) clear sky (b) cloudy sky (c) all sky

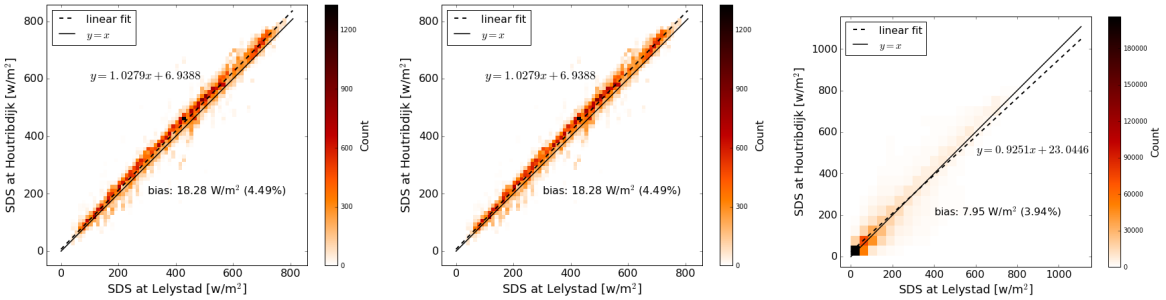

(d) clear sky (e) cloudy sky (f) all sky

Figure A.5: *Comparison scatter plots between ground measurements of Houtribdijk and other stations*

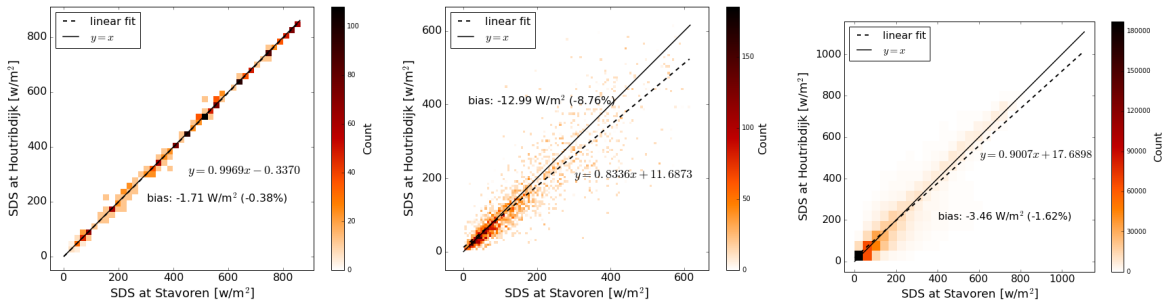

(a) clear sky (b) cloudy sky (c) all sky

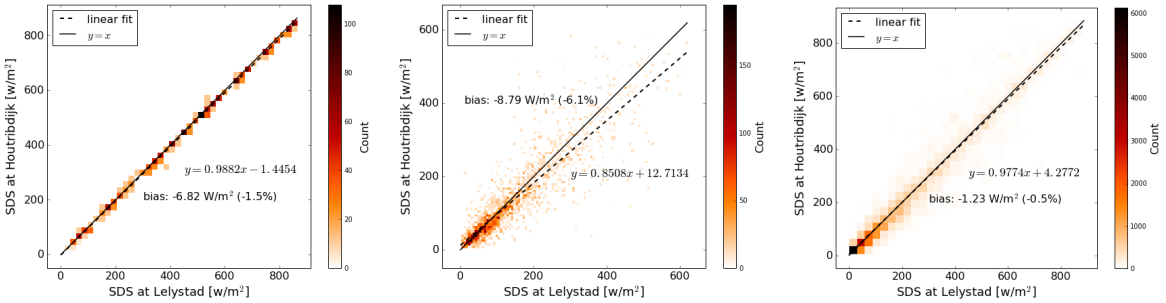

(d) clear sky (e) cloudy sky (f) all sky

Figure A.6: *Comparison scatter plots between satellite observations of Houtribdijk and other stations*